

NASA Technical Memorandum 102488

# Structural Dynamics Branch Research and Accomplishments for FY 1989

*Lewis Research Center  
Cleveland, Ohio*

July 1990

**NASA**

National Aeronautics and  
Space Administration

**Scientific and Technical  
Information Branch**

Trade names or manufacturers' names are used in this report for identification only. This usage does not constitute an official endorsement, either expressed or implied, by the National Aeronautics and Space Administration

## Preface

This document summarizes the technical accomplishments of the Structural Dynamics Branch at the NASA Lewis Research Center for fiscal year 1989. It includes some of the significant results of our in-house researchers, contractors, and grantees.

The Structural Dynamics Branch conducts research dealing with advanced propulsion and power systems as well as precision mechanical systems. Our work directly supports NASA's turboprop, space experiments, space shuttle main engine, national aerospace plane, supersonic fan, space station, and space power programs. This work can be broadly classified into four major activities: turbomachinery aeroelasticity, vibration control, dynamic systems response and analysis, and computational structural methods.

In aeroelasticity, we are developing improved analytical and experimental methods for avoiding flutter and minimizing forced vibration response of aerospace propulsion systems. Work elements include classical (frequency domain) methods, time domain methods, computational methods for fluid-coupled structural response, experimental methods, and application studies (turboprop, turbofan, turbopump, NAVY cruise missile, and advanced core technology). This year we will increase our emphasis on the problems associated with ultra-high-bypass ducted fan aeroelasticity, the aeroelastically forced vibration response of SSME class turbomachinery blading, NAVY cruise missile propulsion, and counter-rotating propfan systems.

In vibration control, we are conceiving, analyzing, developing, and demonstrating new methods to control vibrations in aerospace systems to increase life and performance. Work elements include actively controlled structures, passive vibration control methods, computational methods for active vibration control, and application studies - vibration isolation, piezo-actively and magnetic-controlled bearings, and cryoturbomachinery. In particular, magnetic bearing technology continues to be a major focus for us. For these bearings, methods for unbalance control, critical speed control, and direct control of transient instabilities in rotating equipment are being developed. New approaches for adaptive real-time digital, analog, and hybrid control strategies for active bearing systems are also being developed.

In dynamic systems, we are analyzing and verifying the dynamics of interacting systems as well as developing concepts and methods for motion control in microgravity environs. Work elements include microgravity robotic systems, space mechanisms technology, computational methods for dynamics analysis and application studies - space lab mechanisms and robotics, NASP engine sealing concepts, and parallel computing for dynamics analysis. We are currently greatly increasing our emphasis on developing the basic technology needed for space-based mechanisms in low-earth orbit and high-earth orbit and on lunar and planetary surfaces. Precise, reliable, long-life space-based mechanisms cannot be designed with current technology. Thus, methods for designing and for evaluating the design of such mechanisms will be increasingly important. We are developing technology for reactionless mechanical actuators, precision roller-driven joints for robot arms and other space-based rotary joints, and high-speed, actively controlled bearings for space-based propulsion and pumping systems. We are also developing testing methods for evaluating these new technologies.

Computational methods development has been included in the three other major focus areas within the Structural Dynamics Branch. This work should fundamentally improve the use of modern computers for solving realistic structural dynamics problems, with a particular emphasis on parallel processing. In aeroelasticity, computational methods work is focused on time-domain solutions and coupled fluid structure interaction. In vibration control, the computational methods are focused on individual bearing control, hierarchical schemes for controlling the response of distributed elastic shaft systems, and magnetic vibration isolation of space experiment platforms. In dynamic systems, the focus is on new algorithms for structural dynamics analysis, robot system control, and modeling of NASP engine seals.

As you will read, we have made some exciting accomplishments in fiscal year 1989. We have started some new work and have begun to head in new directions which promise to yield new methods for NASA's missions. Once again, I look forward to next year's accomplishments and to introducing next year's report.

L.L. Kiraly  
Branch Manager

# Contents

Magnetic Suspension Laboratory . . . . .	1
Hybrid Controller for Active Vibration Control . . . . .	4
Active Control of Rotor Vibrations . . . . .	5
Active Control of Flexible Rotor Vibrations by Using Direct Output Feedback . . . . .	8
Tuned Electromagnetic Damper for Cryogenic Turbopumps . . . . .	10
Direct Memory Access Data Transfer Interface With a Transputer Board . . . . .	12
National Aerospace Plane Engine Seal Thermal Analysis at Mach 10 Heat Flux Conditions . . . . .	13
Effect of Axial Vibration on Helicopter Overrunning Clutches . . . . .	16
Survey of Requirements for Microgravity-Experiment Mechanisms . . . . .	18
One-Degree-of-Freedom Reactionless Mechanism . . . . .	19
New Results Concerning the Use of Kinematically Redundant Manipulators in Microgravity Environments . . . . .	21
A Global Approach for Using Kinematic Redundancy to Minimize Base Reactions of Manipulators Used in Microgravity Environments . . . . .	23
Characterization of Structural Connections by Using Free and Forced Response Test Data . . . . .	24
Distributed Finite Element Analysis Using a Transputer Network . . . . .	26
Shape and Topology Optimization by the Homogenization Method . . . . .	28
Parallel Time Integration of Finite Element Problems . . . . .	30
Structural Design of a 6-MW Solar Electric Propulsion (SEP) Spacecraft for Mission to Mars . . . . .	32
Solution and Sensitivity Analysis of a Complex Transcendental Eigenproblem With Pairs of Real Eigenvalues . . . . .	34
Nonlinear Unsteady Supersonic Axial Flow Aerodynamics . . . . .	36
Numerical Analysis of Supersonic Flow Through Oscillating Cascade Sections by Using a Deforming Grid . . . . .	38
Concurrent Processing Adaptation of Aeroelastic Analysis of Propfans . . . . .	40
Flutter Analysis of Supersonic Throughflow Stator . . . . .	41
Appendix - Researchers . . . . .	42
Bibliography . . . . .	43

# Magnetic Suspension Laboratory

A laboratory has been established to research magnetic suspension of turbomachinery shafts and acceleration-sensitive experiments for space applications. Magnetic bearings have been shown in ground-based applications to have significant advantages - including the elimination of wear (and the need for lubrication systems); higher shaft speed limits; control of stiffness-to-shift resonances; and control of damping to reduce resonant, transient, and subsynchronous vibration. Turbofan engines and space turbopumps could both benefit from magnetic bearings. Magnetic suspension appears to offer the best way to achieve the extremely soft support needed for microgravity experiments and production processes, such as crystal growing, in space.

The 2-year-old laboratory (fig. 1) is now equipped with a considerable array of magnetic actuators, control systems, power supplies, test fixtures, fast control compu-

ters, and various support electronics. A three-degree-of-freedom testbed (fig. 2) measures the degree of vibration transmitted from a vibrating support to the suspended structure. This system is levitated with a digital control system, linear power supplies, and several magnetic actuators. In cooperation with the Space Experiments Division, it is being extended to a full six-degree-of-freedom suspension system.

The first NASA Lewis Research Center (fig. 3) magnetic bearing has been operated to 12 000 rpm with a digital control loop. (Most magnetic suspension systems are inherently unstable except when placed under closed-loop control.) Figures 4 and 5 illustrate two primary advantages of magnetic bearings - the ability to alter shaft critical speeds by changing the bearing stiffness (fig. 4) and the ability to control damping to reduce shaft vibration amplitude (fig. 5).



FIGURE 1. - MAGNETICS LABORATORY.

ORIGINAL PAGE  
BLACK AND WHITE PHOTOGRAPH

ORIGINAL PAGE  
BLACK AND WHITE PHOTOGRAPH

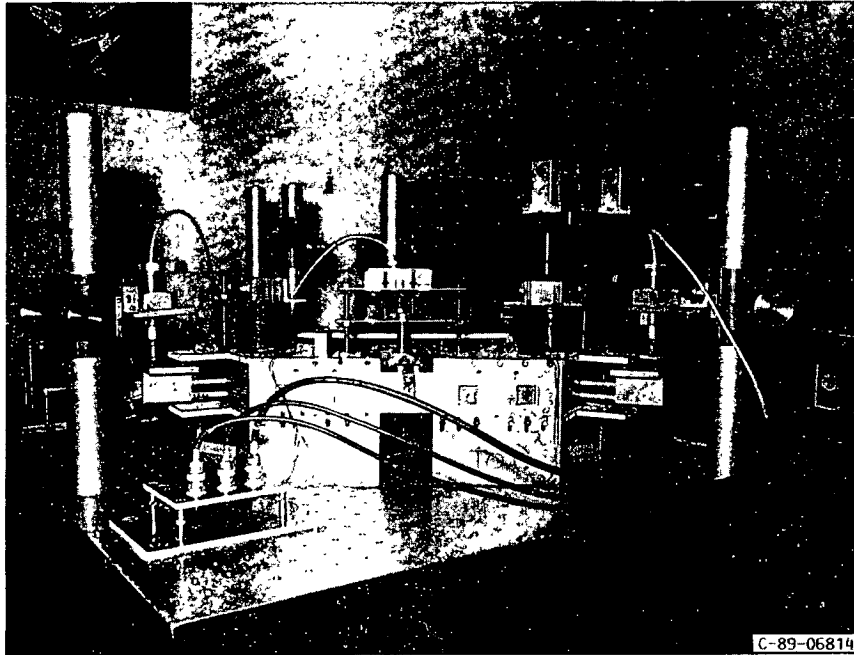


FIGURE 2. - THREE-DEGREE-OF-FREEDOM LEVITATED PLATFORM.

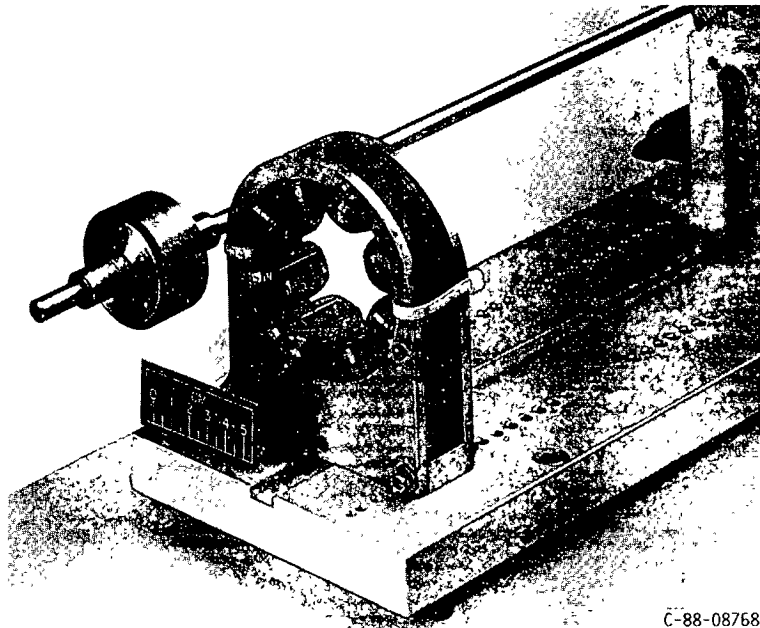


FIGURE 3. - MAGNETIC BEARING.

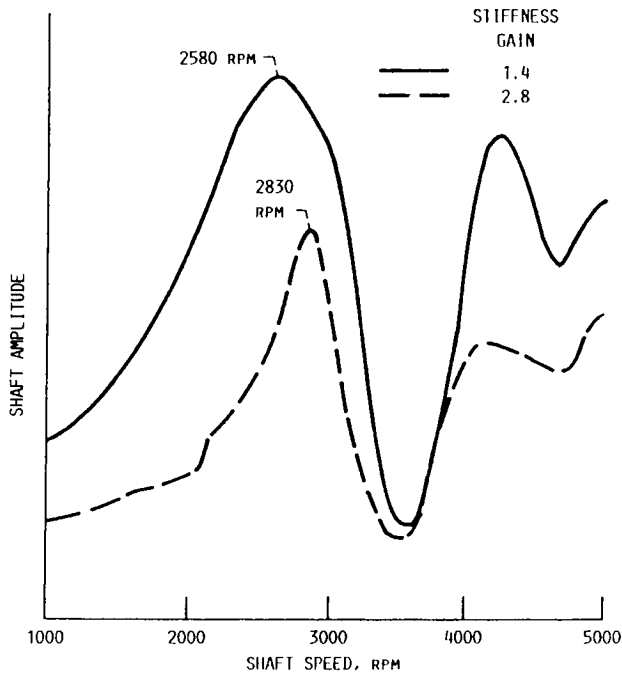


FIGURE 4. - CHANGING SHAFT CRITICAL SPEED.

Magnetic bearing program goals include (1) significant performance increases (15-percent increase in fuel consumption efficiency) and weight reduction (5 percent) for turbofan engines and (2) a tenfold increase in time before overhaul for space turbopumps. The near-term research goals include (1) increasing the strength of the magnetic bearing actuator by using higher saturation materials and more compact designs (surpassing the pressure exerted by fluid film bearings) and (2) reducing the size and weight of the control systems and power supplies.

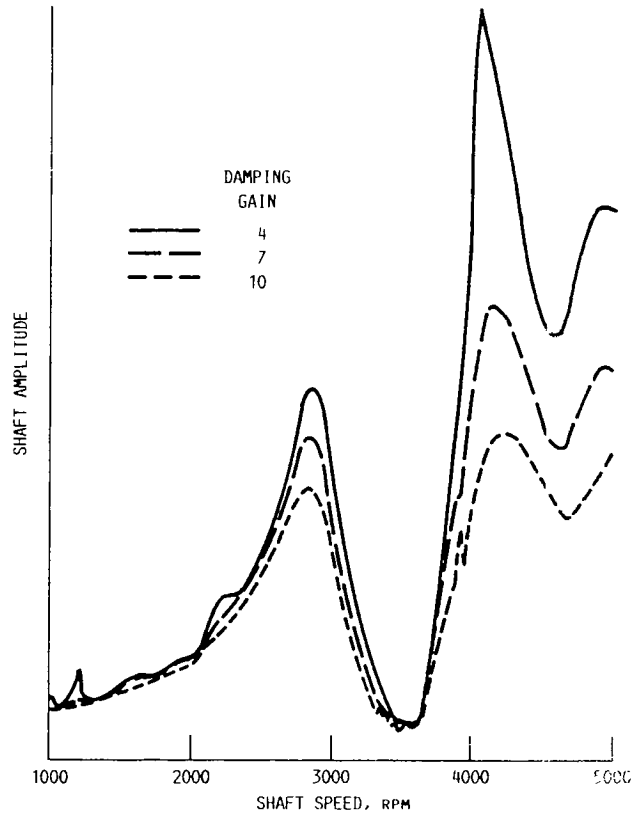


FIGURE 5. - CHANGING BEARING DAMPING.

**Researchers:** G.V. Brown, D.P. Fleming, C.M. Grodsinsky, E.H. Meyn, and S.J. Posta (NASA Lewis), and C.T. Finlay (Sverdrup).

# Hybrid Controller for Active Vibration Control

A unique controller was recently developed by the Technical University of Munich, Institute of Mechanics, for systems requiring active vibration control. The controller employs 12-bit digital-to-analog (D/A) converters (DAC's) that are capable of full four-quadrant multiplication. The analog output signal from these DAC's is derived from a conventional R-2R current-switching ladder network, and this signal is directly proportional to the product of the applied reference voltage and a digital input word. If an analog signal anywhere in the range from -10 to 10 V is applied to the reference voltage terminals and the value of the digital input is in the range of -1 to 1, the output signal can have any value from -10 to 10 V. Thus each DAC acts as a digitally controlled attenuator since the analog output amplitude is dependent on the value of the digital input word. The controller is classified as a hybrid because its output responds to both analog and digital inputs.

The controller employs eight DAC's on a printed circuit board (fig. 6). The controller also has a summing circuit with eight inputs, one from each DAC output. The DAC outputs are combined by the summing circuit to give a composite analog output. Following the summing circuit is an active low-pass filter circuit that attenuates any high-frequency noise and switching transients appearing at the output of the summing circuit. Triple-state latches are used to isolate the digital control inputs from the DAC circuitry and to reduce high-frequency noise, which can be coupled to sensitive analog circuitry.

The analog output from the controller can be used in a feedback loop to drive magnetic bearings or electromagnetic, piezo, or hydraulic actuators. The feedback signal is a composite of the analog signal input to each DAC. Inputs such as a displacement measurement and its associated velocity, acceleration, and integral components can be digitally blended to optimize the output for minimum vibration amplitudes.

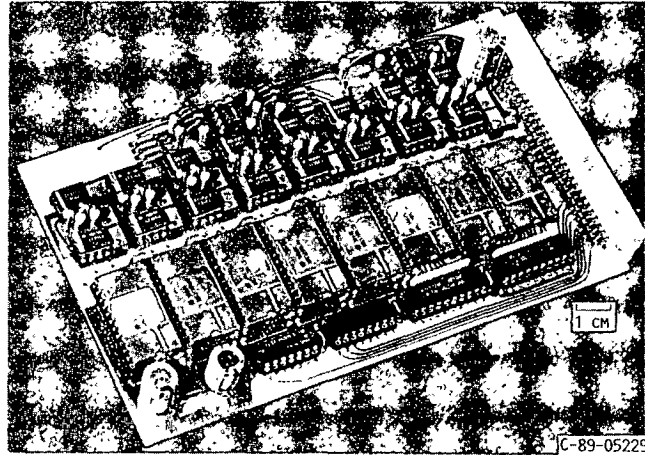


FIGURE 6. - DIGITAL-TO-ANALOG CONVERTER ARRAY BOARD.

The features of the hybrid controller will be adapted for research projects in the magnetic suspension laboratory at NASA Lewis - the magnetic suspension of turbomachinery shafts and the control of acceleration-sensitive experiments in space. Initial studies are planned to involve a hybrid controller system employing four controller boards for two magnetic bearings that support an elastic rotor. The goal will be to demonstrate that feedback components - such as system stiffness, damping, mass or inertia, and radial displacement - can be optimized in this application.

---

**Researchers:** H. Ulbrich (Technical University of Braunschweig), G.V. Brown and S.J. Posta (NASA Lewis), and C.T. Finlay (Sverdrup).

# Active Control of Rotor Vibrations

Currently, jet engine shaft vibrations are suppressed by passive devices such as squeeze film dampers. Research is being performed to replace or supplement these with active dampers to reduce engine weight and produce more predictable and reliable damping. Piezoelectric pushers are used as actuators in these active dampers because of their light weight, compactness, and low voltage.

Tests were conducted to determine if active damping control with piezoelectric pushers could suppress vibration of an air-turbine-driven overhung rotor rig (fig. 7). The results showed that high-frequency electromechanical instabilities occurred if no electrical filters were included in the feedback loop. However, the insertion of low-

pass electrical filters did not prevent their instabilities but only changed their frequencies.

Component testing pinpointed the cause of the electromechanical instabilities to be phase lags in the piezoelectric actuators, in the electrical filters, and in the differentiator used to obtain a velocity signal in the active damper feedback loop. A subsequent test was run on the overhang rotor test rig after the electrical circuits were redesigned to minimize phase lag effects. These modifications minimized the instabilities.

Increasing the gain in the active damper feedback loop significantly reduced the bearing housing response to disk unbalance (fig. 8). The active damper reduced the

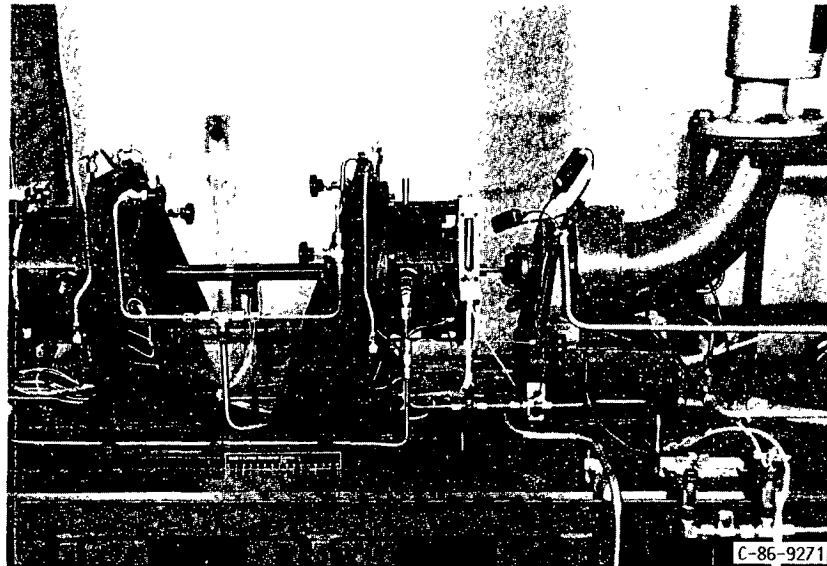


FIGURE 7. - HIGH-SPEED TRANSIENT DYNAMICS RIG FOR ACTIVE ROTOR VIBRATION CONTROL.

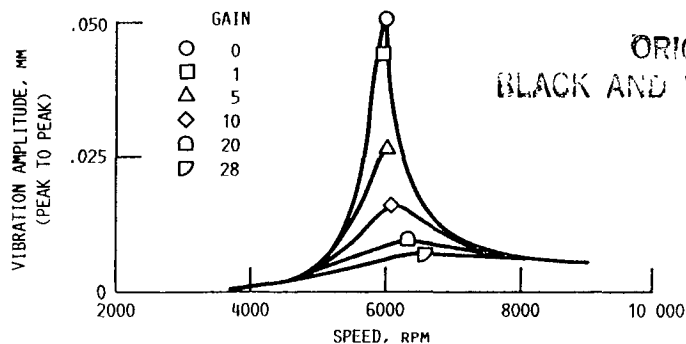


FIGURE 8. - OUTBOARD BEARING HOUSING VIBRATION VERSUS FEEDBACK GAIN.

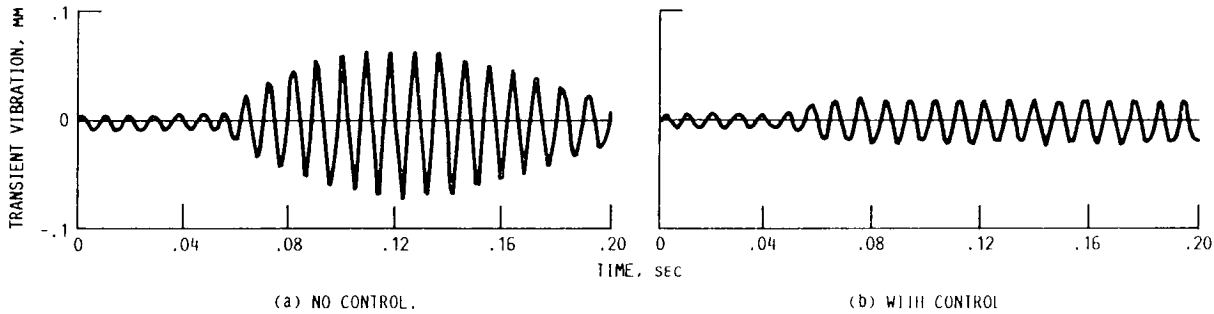


FIGURE 9. - EXPERIMENTAL TRANSIENT RESPONSE - SUDDEN BOLT LOSS. OUTBOARD DISK IMBALANCE, 0.19 G (43.01 MM) - 8.17 G-MM; SPEED, 6600 RPM. CRITICAL SPEED, 6400 RPM

critical speed response by a factor of 6 and held this reduction for 30 hr (10 million cycles) nonstop. The pusher tip temperature was measured immediately after the test and found to be only 86 °F. The maximum stroke of the pusher is about 3.0 mil (peak to peak), and some problems occurred when these limits were exceeded. Next the active damper's ability to suppress vibration due to a sudden mass unbalance on the disk was demonstrated by using a solenoid-driven plunger to shear off a rotating bolt on the disk. The active damper effectively controlled this type of vibration (fig. 9). The active damper also suppressed subsynchronous vibration. For this test, the disk was encased by an annular ring with a small clearance. Oil was allowed to drain into the clearance to induce oil whirl. The subsynchronous vibration was significantly reduced with increasing values of feedback gain in the active damper.

An active stiffness feedback loop was constructed with the pusher internal motion proportional to the bearing housing motion. The active stiffness was used to shift the critical speed between the two extremes (fig. 10). A critical speed can be almost totally avoided by switching the active stiffness feedback gain from 20 to 0 during the coastdown (fig. 11).

Finally, it was demonstrated that the active damper could still attenuate vibrations if a significant change occurred in the mass of the rotor. The total weight of the outboard disk was reduced from 3.21 to 1.39 lb. The active damper still damped

the vibrations of the modified system, which exhibited an extremely large response at the first critical vibration when the active damper ( $G = 0$ ) was not used. The extent of the system modification is indicated by the increase in critical speed - from 65 000 rpm (original rotor) to 75 000 rpm (modified rotor).

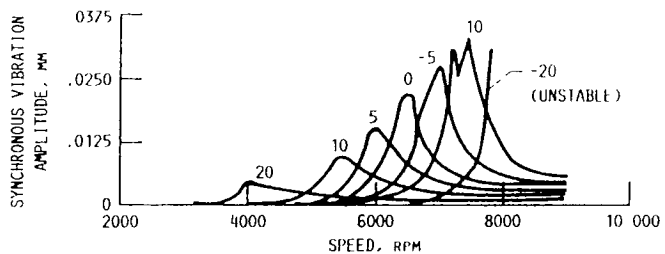


FIGURE 10. - RESPONSE AMPLITUDE (FIRST DEGREE OF FREEDOM, NODE 1) VERSUS GAIN. NUMBERS INDICATE GAIN.

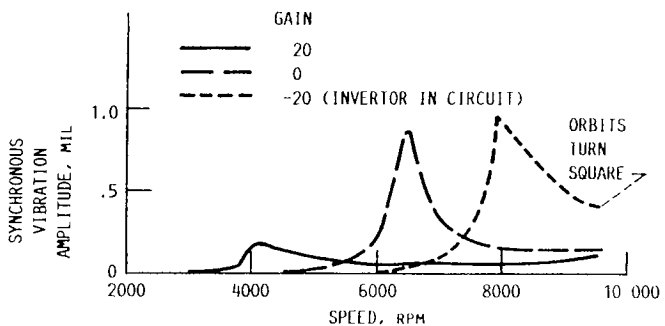


FIGURE 11. - RESPONSE TO EXTREME VALUES OF ACTIVE STIFFNESS.

Future plans for the project include the following:

- (1) Working with the piezoelectric pusher manufacturer to develop high-temperature actuators with increased stroke and force, and decreased phase lag and voltage
- (2) Testing piezoelectric actuator components to determine how their phase lag varies with their structural and electrical characteristics
- (3) Designing special pusher brackets and pushers to avoid instability
- (4) Determining T700 engine applications for the piezoelectric actuator specifications-based active damper/spring

- (5) Performing simulations to determine if control algorithms that use linear combinations of active stiffness and damping can reduce vibration sufficiently with smaller stroke requirements than uncoupled active dampers or stiffnesses
- (6) Developing modal identification algorithms that use piezoelectric pushers to obtain the modal characteristics of the rotor-bearing system

---

**Researchers:** A.F. Kascak (AVSCOM), A.B. Palazzolo and R.R. Lin (Texas A&M), G.T. Montague (Sverdrup), and J.J. Ropchock and T.F. Lakatos (NASA Lewis).

# Active Control of Flexible Rotor Vibrations by Using Direct Output Feedback

Experiments were performed to actively control the rotor vibrations of a flexible rotor mounted on flexible bearing supports. The active control method used in the tests is called "Optimal Direct Output Feedback Control." Four electrodynamic actuators apply control forces directly to the bearing housings to effectively control the rotor vibration. The force actuators are controlled by an analog controller that accepts rotor displacements as input; the controller is programmed with experimentally determined feedback coefficients; and the output is a control signal to the force actuators.

The tests were carried out on the rotating systems dynamics rig (fig. 12). With

the control system turned off, there were nine resonances between 0 and 10 000 rpm. Rotor amplitudes are shown as a function of speed in figure 13. With no control, vibration amplitudes were as high as 300  $\mu\text{m}$ . The actuators provided significant passive damping even when the controller was inactive. The active controller reduced the vibration amplitude considerably from the passive damping case. The resonances were no longer evident, and the rotor amplitude was never more than 25  $\mu\text{m}$ . Unlike passive vibration control, active vibration control reduced vibration at the resonances without increasing it at off-resonance conditions.

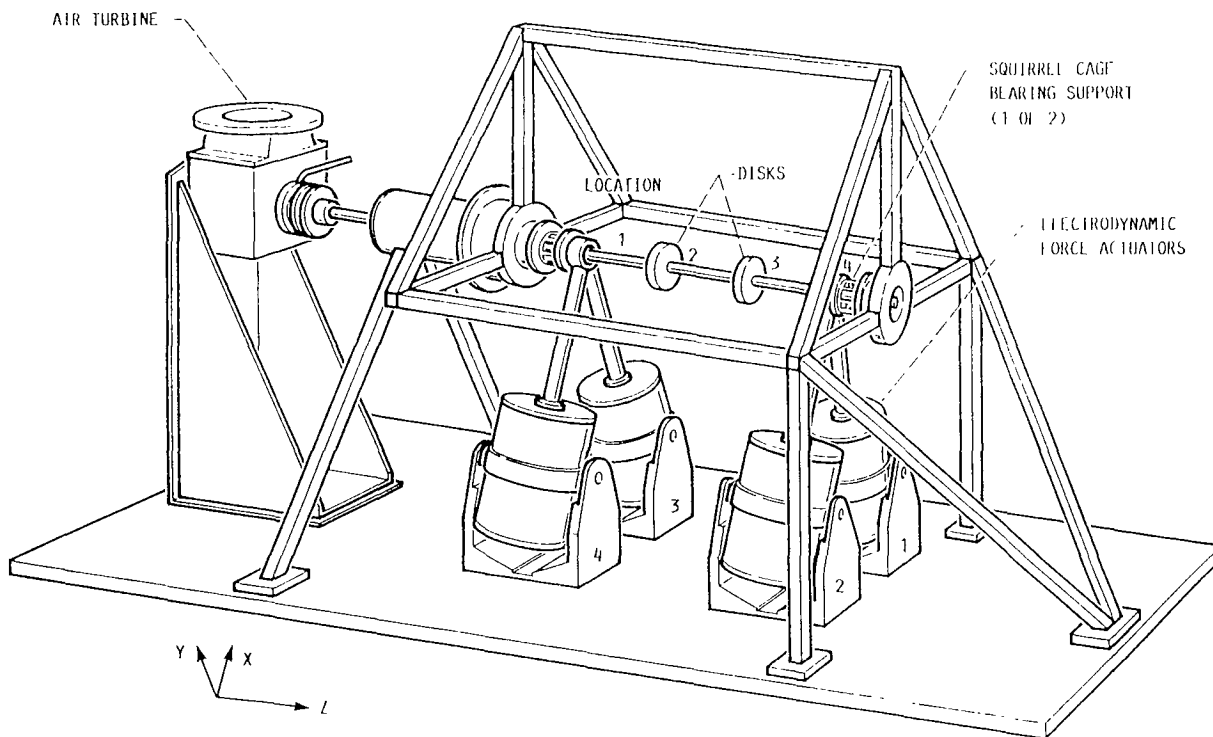


FIGURE 12. - ROTATING SYSTEMS DYNAMICS RIG. CHARACTERISTICS OF ELECTRODYNAMIC FORCE ACTUATORS: VELOCITY, 1.78 M/SEC. FREQUENCY, 7000 HZ; FORCE, 445 N; DISPLACEMENT, 6.35 MM.

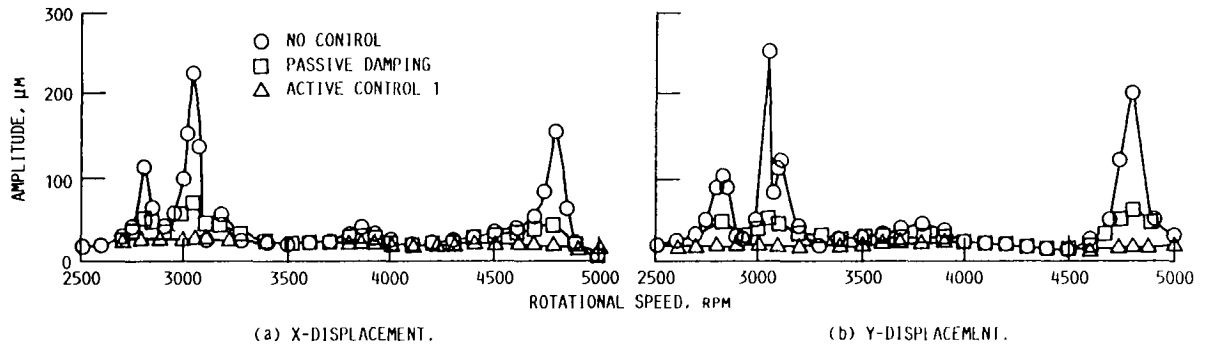


FIGURE 15. - EXPERIMENTAL UNBALANCE RESPONSE FOR NO CONTROL, PASSIVE DAMPING, AND ACTIVE CONTROL 1.

**Researchers:** K. Nonami (Chiba University) and E. DiRusso and D.P. Fleming (NASA Lewis).

# Tuned Electromagnetic Damper for Cryogenic Turbopumps

The tuned electromagnetic damper is a device that damps rotor vibrations in cryogenic environments such as liquid oxygen or liquid hydrogen turbopumps for rocket engines. The damper requires very cold temperatures, of the order of  $-300^{\circ}\text{F}$ , in order to be effective. The low temperatures inherent in cryogenic turbopumps make this damper very well suited to cryogenic applications.

The basic components of the tuned electromagnetic damper are shown in figure 14. These are the copper coils, neodymium-iron-boron magnets, and magnetic iron. Another key component of the damper is a capacitor (not shown in

fig. 14). The coils are fastened to a carrier plate that is rigidly attached to the bearing housing, and they are situated within the magnetic field produced by the magnets located above and below the coils.

The electrical circuit for the tuned electromagnetic damper is shown in figure 15. The copper coils provide the resistance and inductance, and the capacitor enables the circuit to be tuned to generate maximum current (resonate) at the mechanical vibration frequency. Two such circuits are required for the damper - one for the x-axis and one for the y-axis. The two circuits are electrically independent of each other.

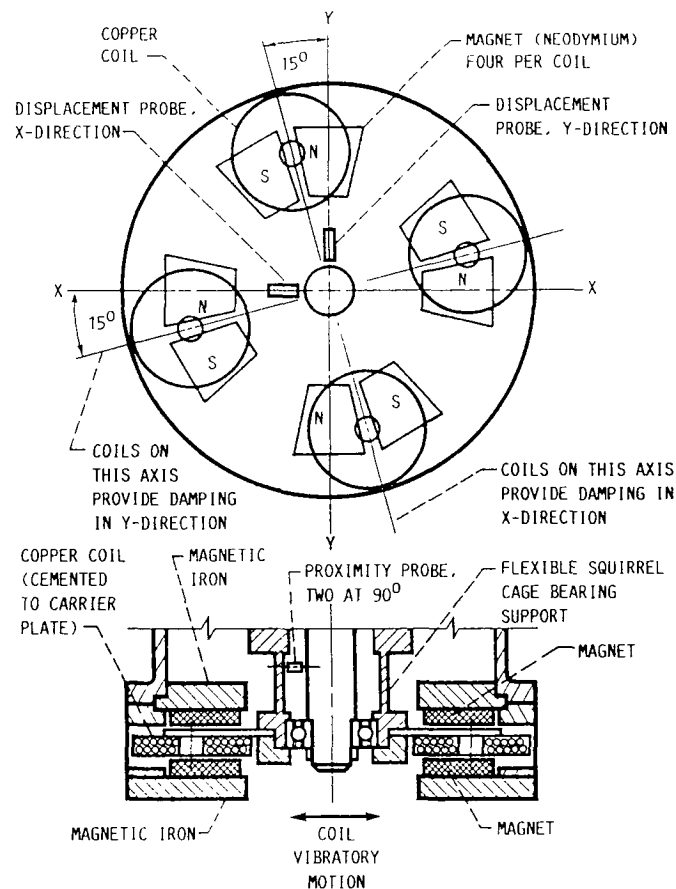


FIGURE 14. - SKETCH OF ELECTROMAGNETIC DAMPER SHOWING ARRANGEMENT OF COPPER COILS, MAGNETS, AND DISPLACEMENT PROBES.

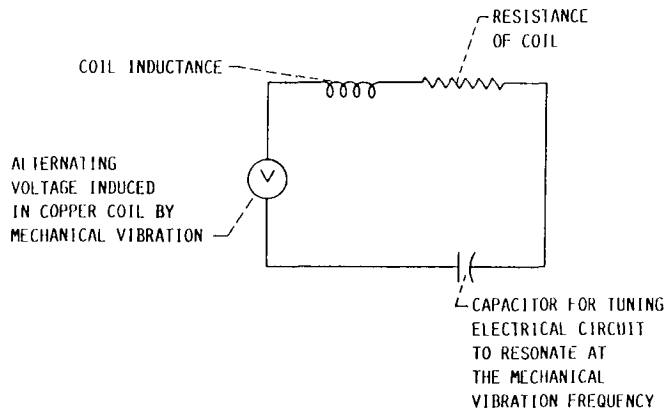


FIGURE 15. - TUNED ELECTRICAL CIRCUIT SCHEMATIC. POWER DISSIPATED IS  $P = I^2R$ , WHERE  $I$  = CURRENT FLOW IN COIL AND  $R$  = RESISTANCE OF COIL.

Vibratory motion of the coils (fig. 14) within the magnetic field induces an alternating voltage in the coils, and an alternating current then flows in the circuit. The frequency of the alternating voltage and current is equal to the frequency of the vibratory motion.

Because of their resistance, the coils are heated by the current flowing through them. This heat is dissipated to the surroundings, thus damping the vibratory motion. The power dissipated is proportional to the square of the current generated in the electrical circuit. Therefore, the electrical circuit must be tuned so that its resonant frequency equals the rotor vibration frequency. Tuning results in maximum current flow in the circuit and hence maximum damping. The resonant frequency of the circuit is set equal to the vibration frequency of the rotor by selecting the value of the capacitor in the circuit.

The damping coefficient  $c$  as a function of damper variables is given by the following equation:

$$c = \frac{N^2 \beta^2 \ell^2 R}{R^2 + \left( 2\pi fL - \frac{1}{2\pi fC} \right)^2} \text{ N sec/m}$$

where

- $N$  number of conductors in flux path
- $\beta$  flux density, Weber/m<sup>2</sup>
- $\ell$  length of conductor, m
- $R$  resistance of the coils,  $\Omega$
- $f$  frequency of vibration, Hz
- $L$  inductance of coils, H
- $C$  capacitance of circuit, F

Figure 16 compares the undamped and damped amplitude response for a test rotor at liquid nitrogen temperature (-321 °F).

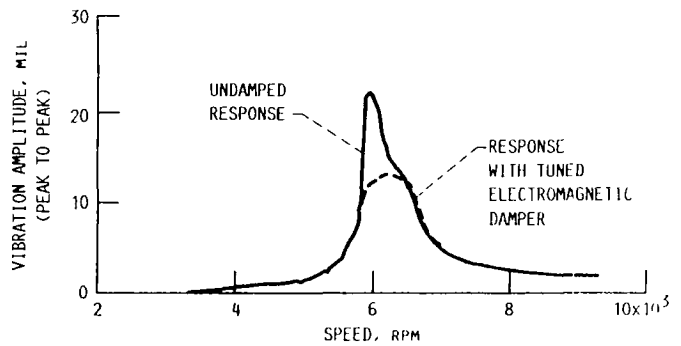


FIGURE 16. - COMPARISON OF UNBALANCE RESPONSE IN Y-DIRECTION WITH AND WITHOUT ELECTROMAGNETIC DAMPER.

**Researchers:** E. DiRusso and G.V. Brown (NASA Lewis).

# Direct Memory Access Data Transfer Interface With a Transputer Board

An IBM PC-AT based interface to an INMOS IMS B008 transputer board (also installed in the AT) has been developed (fig. 17). The IMS B008 board has a direct memory access (DMA) interface and interrupt capabilities that were unavailable on earlier INMOS transputer boards. Previously, the simplest and only data transfer method available was polling. DMA can provide higher data transfer rates. In addition, the use of interrupts makes it unnecessary for the AT to continuously poll the B008 status registers. The AT host computer can be working on something else while the transputer is running. When the transputer has completed its task, the AT can be interrupted and the necessary information received from the transputer.

The AT program is written in Pascal, whereas the transputer program is written in OCCAM, a language developed specifically for the transputer. The Pascal program initializes the registers of the DMA controller on the AT with the necessary information including the starting address of the

data block and the size of the data block. The data are then transferred to the transputer where they are received by the OCCAM program. When the data transfer is complete, the AT can work on a new task while the transputer works with the data it has just received. The transputer signals when it is ready to output data back to the AT, perhaps after calculating new values. The interrupt causes a service routine to be called. After the service routine ends, the AT can continue its interrupted task.

The DMA interface will enable the transputer to control a real-time system. One such system being considered is a magnetic bearing control program. In this system the OCCAM code will calculate new controller biases and gains, while the Pascal code retrieves those values to update information on a status screen. DMA transfers and interrupts will be used in this system to see if they are more beneficial and efficient than the polling process currently being used.

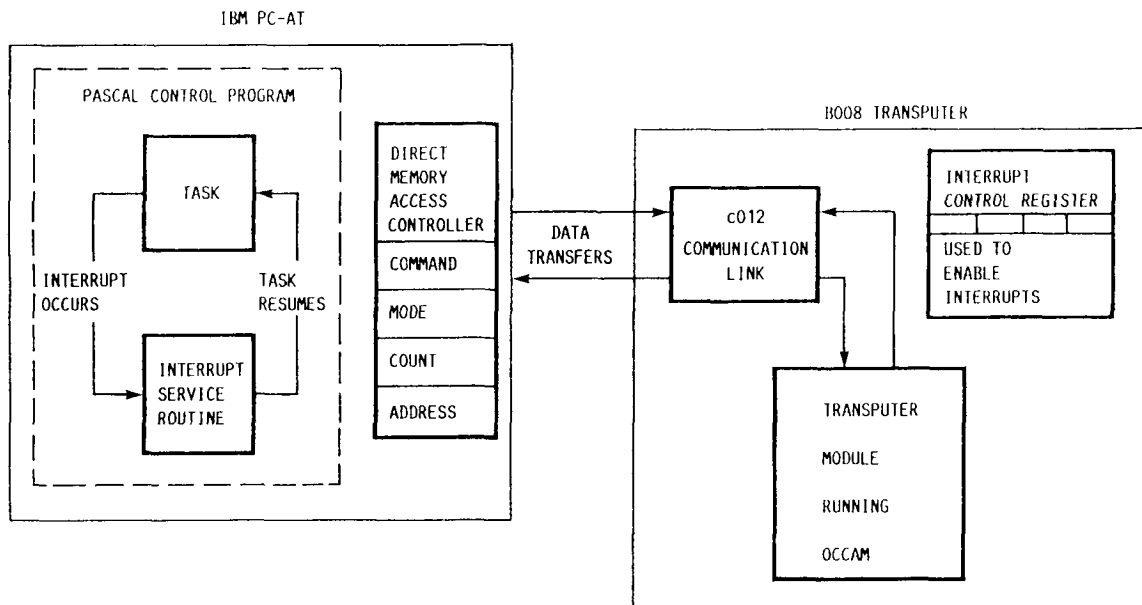


FIGURE 17. - IBM PC-AT/B008 INTERFACE DIAGRAM.

**Researchers:** M. Babula (University of Toledo), C.T. Finlay (Sverdrup), and L.J. Kiraly and D.C. Janetze (NASA Lewis).

# National Aerospace Plane Engine Seal Thermal Analysis at Mach 10 Heat Flux Conditions

A critical mechanical system in advanced hypersonic engines is the panel-edge seal system that seals gaps between the articulating engine panels and the stationary engine splitter walls. These seals must prevent the extremely hot, pressurized engine flow-path gases from escaping past the movable panels.

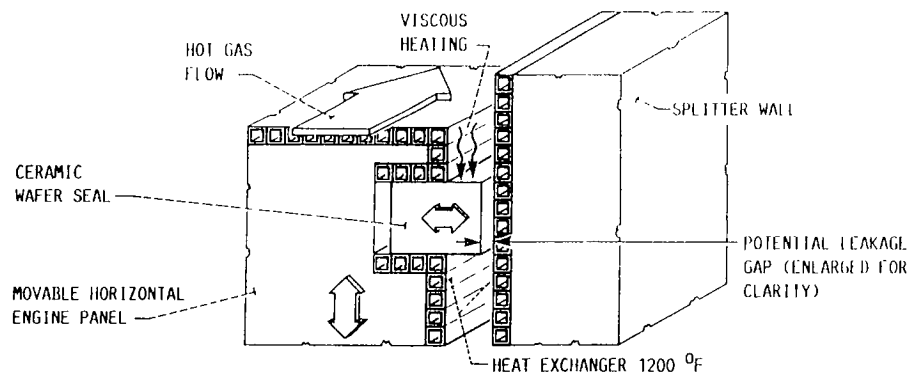
Engine chamber temperatures and pressures vary significantly with axial engine station, vehicle speed, ramjet or scramjet cycle, and fuel-to-air ratio. Calculations were made at NASA Lewis to estimate the flow-path pressures and temperatures of a generic hypersonic engine flying a (1500-lb/ft<sup>2</sup>) flight trajectory. In this study, one of the most punishing conditions for the seals occurred at Mach 10 - where pressure differentials reached 85 psi, engine static temperatures reached 4900 °F, and combustor entrance heat flux rates reached 1160 Btu/ft<sup>2</sup>/sec.

The objective of the current research was to numerically assess the ability of a National Aerospace Plane (NASP) engine panel-edge seal (under engine-simulated heat fluxes) to seal the high-temperature,

pressurized flow-path gases. A ceramic wafer seal developed at NASA Lewis was considered.

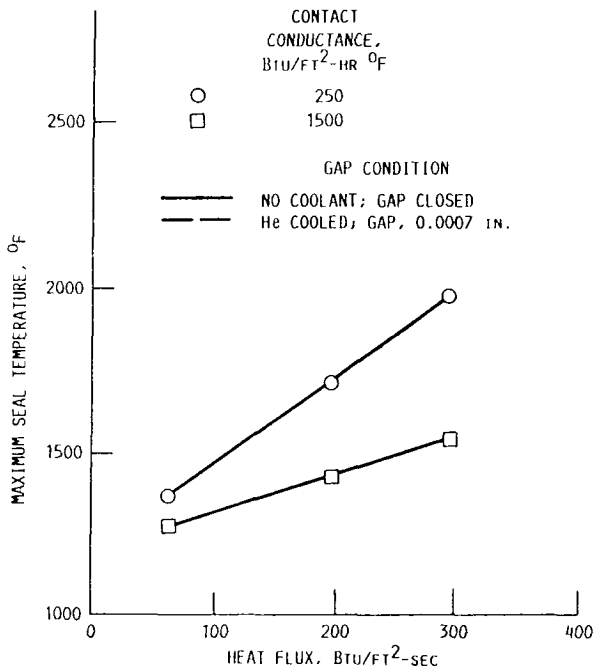
The seal's temperature dependence on (1) viscous heating, (2) surface contact conductance between the seal and its adjacent surfaces, (3) flow of purge coolant gases, and (4) leakage of hot engine flow-path gases was examined from the engine inlet back to the entrance region of the combustion chamber. The boundary conditions considered for the seal are shown schematically in figure 18. The gap between the seal nose and the adjacent wall was modeled in three modes: (1) closed with no leakage of gases, (2) purged with a coolant gas, and (3) open with a small leakage of flow-path gases.

Using the coupled finite element/finite difference approach developed, a parametric study evaluated maximum seal temperatures over a range of simulated engine inlet heat flux rates (60 to 300 Btu/ft<sup>2</sup>/sec) for two different surface contact conductances (fig. 19(a)). The two contact conductances considered (250 and 1500 Btu/ft<sup>2</sup>/hr/°F)

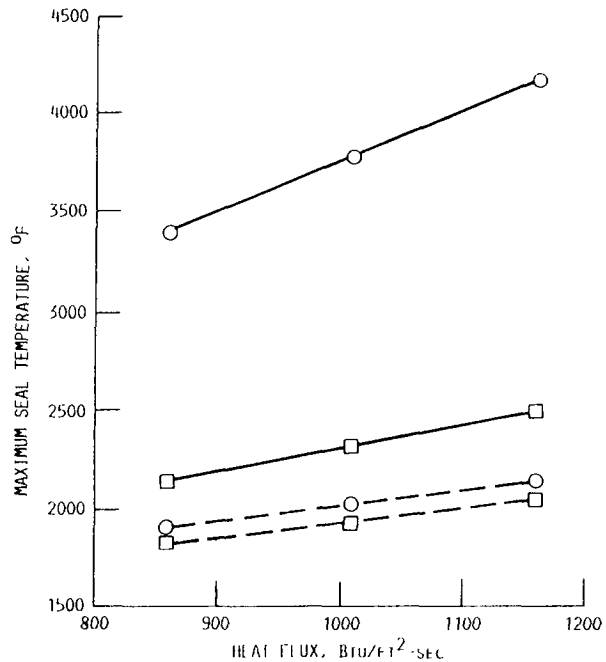


GAP CONDITIONS	THERMAL BOUNDARY CONDITIONS
CLOSED	CONDUCTION: CONTACT CONDUCTANCE (250 OR 1500 Btu/ft <sup>2</sup> -HR °F)
PURGED WITH HELIUM GAS	GAS COOLS SEAL; THERMAL RADIATION BETWEEN SEAL NOSE AND SIDEWALL
SMALL LEAKAGE OF FLOWPATH GAS	LEAKAGE GAS HEATS SEAL; THERMAL RADIATION BETWEEN SEAL NOSE AND SIDEWALL

FIGURE 18. - SUMMARY OF THERMAL ANALYSIS BOUNDARY CONDITIONS.



(a) MAXIMUM SEAL TEMPERATURE FOR ENGINE INLET HEAT FLUX RATES FOR TWO SURFACE CONTACT CONDUCTANCES. GAP CLOSED



(b) MAXIMUM SEAL TEMPERATURE FOR COMBUSTOR ENTRANCE REGION HEAT FLUX RATES FOR TWO SURFACE CONTACT CONDUCTANCES. CASE 1. GAP CLOSED, NO COOLANT. CASE 2. SMALL GAP, He PURGE COOLANT.

FIGURE 19. - MAXIMUM CERAMIC WAFER SEAL TEMPERATURE FOR ENGINE INLET AND COMBUSTOR ENTRANCE REGION HEAT FLUX RATES

represent a range of conductances typical of ceramic-to-metal contacts. (Surface contact conductance controls the rate at which heat transfers across the ceramic-to-metal interfaces.) The results shown for the closed-gap condition indicate that even with the poorest contact conductance considered, the maximum seal temperature for the 300 Btu/ft<sup>2</sup>/sec was less than 2100 °F. This maximum seal temperature was below the 2500 °F maximum allowable operating temperature for silicon carbide ceramic wafers. Similar results were obtained for the case in which engine inlet gases were allowed to flow through a small leakage gap. Because the ambient flow-path temperatures in the engine inlet were not severe, only a small increase in seal temperature was observed. For Mach 10 operation, it was determined that active cooling of the seals alongside the engine inlet ramp would not be required.

A similar parametric study was conducted to assess the maximum seal temperatures at axial engine stations leading to the combustor entrance region. The upper two curves shown in figure 19(b) depict the

seal temperatures for the case in which the gap between the seal nose and the adjacent panel is closed. The results demonstrated the sensitivity of the maximum seal temperature to the contact conductance. For good surface conductance (the lower curve) the maximum seal temperature was below the allowable operating temperature of 2500 °F for heat fluxes up to 1130 Btu/ft<sup>2</sup>/sec. However, for low contact conductance, the maximum seal temperature exceeded the allowable operating temperatures for all of the combustor entrance heat flux rates considered.

For conditions in which the calculated seal temperatures exceeded the seal allowable temperature, some form of active coolant was required. Cooling the seals with a positive purge of an inert gas offered two attractive features. First, a positive flow of gas from the backside engine cavity past the seal and into the engine cavity cools the seals. Second, maintaining a positive purge of an inert gas (such as helium) past the seals greatly reduces the risk of explosive mixtures of hydrogen and oxygen leaking past the engine panels.

The seal temperatures of the lower two curves of figure 19(b) are calculated with a small flow rate of 70 °F helium, 15 psi above local engine flowpath pressure flowing from the backside of the seal past the seal nose into the engine flowpath. As can be seen in the figure, the maximum temperature of the seal was lowered to below the 2500 °F over the wide heat flux range considered. The purge coolant effects on the hot seal were determined with a specially developed one-dimensional, compressible flow code that accounted for the effects of heat transfer, friction, and variable

gas properties. The LEAK finite difference code was run iteratively with MARC (a general purpose finite element code) to predict temperature distributions within the seal. The solution converged to the final seal temperatures when the seal boundary and leakage gas were in thermal equilibrium.

---

**Researchers:** B.M. Steinetz (NASA Lewis), M. Tong (Sverdrup), and W.J. Coirier (NASA Lewis).

# Effect of Axial Vibration on Helicopter Overrunning Clutches

A sprag overrunning clutch is an integral part of a helicopter's drive train. It transmits torque from the engine to the combining gearbox and overruns when the gearbox rotates faster than the engine. Sprag clutches operate on the wedging action of a small sprag located between the inner and outer race. Engagement occurs when relative motion between the two races forces the camlike sprag to a more upright position. Many clutch engagement failures have occurred while the second turbine was being brought on-line under vibratory conditions. Tests were conducted to determine the axial vibratory load which would induce slippage in an engaged clutch.

Figure 20 is a drawing of the fixture used to perform the tests. The top flange

was rigidly mounted to the top of the MTS machine, and the bottom flange acted as a coupling to the machine's actuator (fig. 21). The coupling transmitted axial and torsional forces to the clutch. Because of the design of the fixture, relative motion could only occur at the contact point between the inner race and the sprags.

Three clutch configurations were tested: a single Formsprag clutch (SF), a double Formsprag clutch (DF), and a Borg-Warner clutch (BW). The SF clutch consists of sprags positioned in a single cage, the DF clutch consists of two SF clutches in parallel, and the BW clutch incorporates two rows of sprags in a single housing. These configurations were tested at 80, 100, and 110 percent of rated torque capacity.

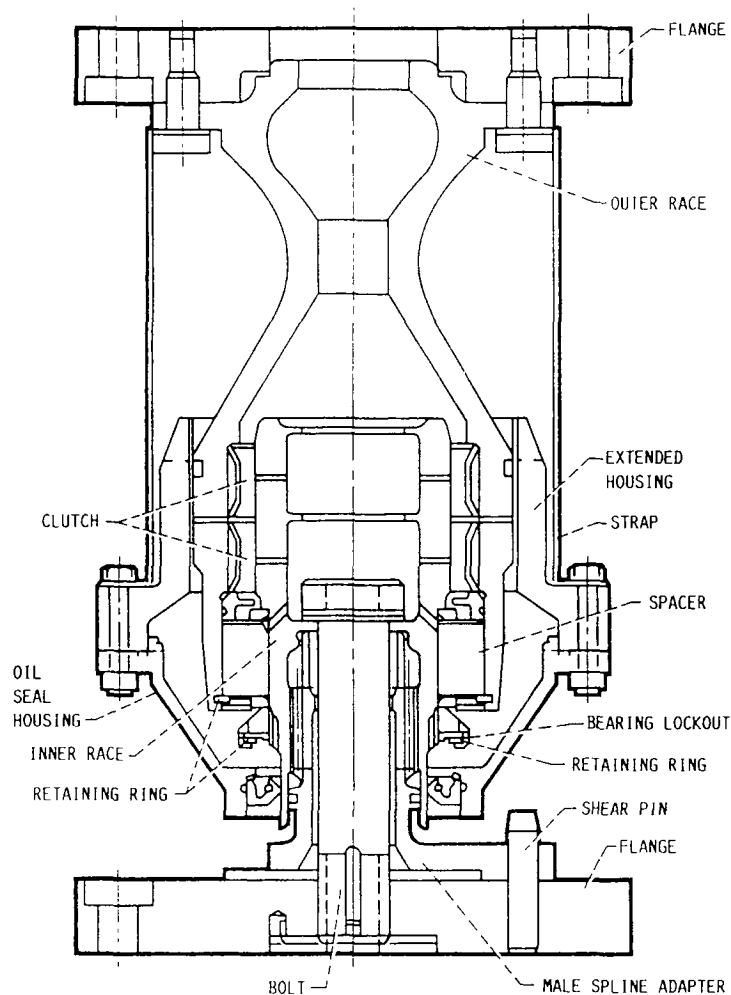


FIGURE 20. - DIAGRAM OF TEST FIXTURE WITH DESCRIPTION OF COMPONENTS.

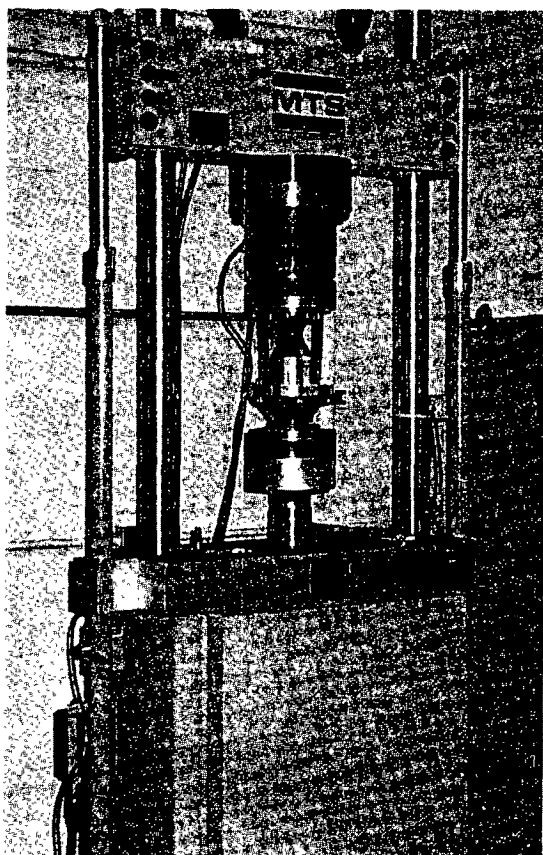
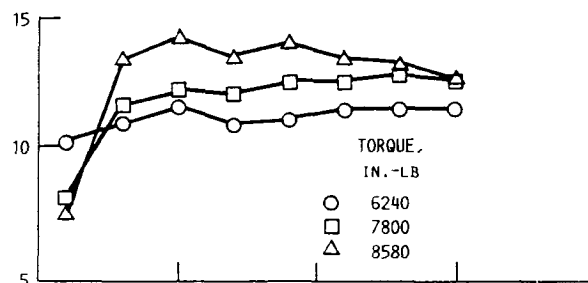


FIGURE 21. - MOUNTING OF TEST FIXTURE.

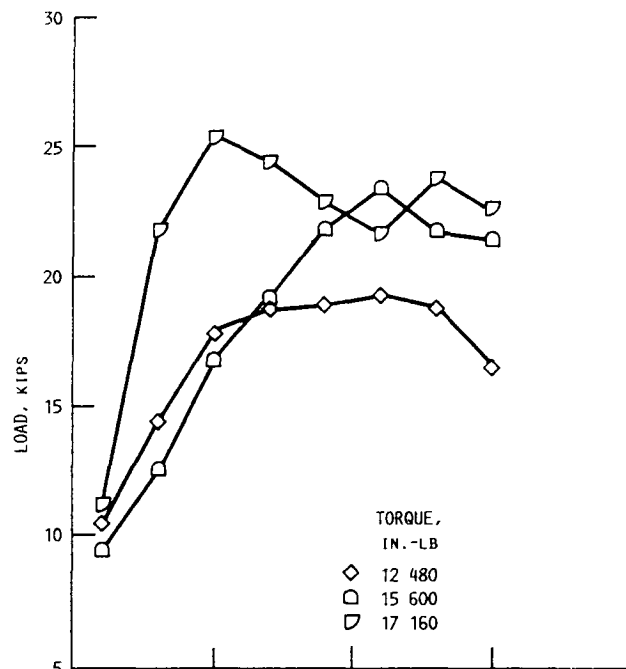
For each torsional load, axial frequencies of 1, 3, 5, 7, 9, 11, 13, and 15 Hz were applied. Amplitude values for each frequency were manually adjusted until slippage occurred.

For the SF clutch, the axial vibration range which produced slippage was from 8 to 14 kips at all frequencies tested (fig. 22). The normal force increased as the torque increased for all configurations. Comparison of the SF and DF graphs shows that the addition of a second clutch did not double the force necessary for slippage. The DF's wide spread of values, from 9 to 25 kips, was due to a nonuniform load distribution between the two rows of sprags. Furthermore, the DF and BW graphs indicate that the BW single-cage design reduces the force necessary for slippage because of a greater nonuniform load distribution, even though these configurations have the same number of sprags.

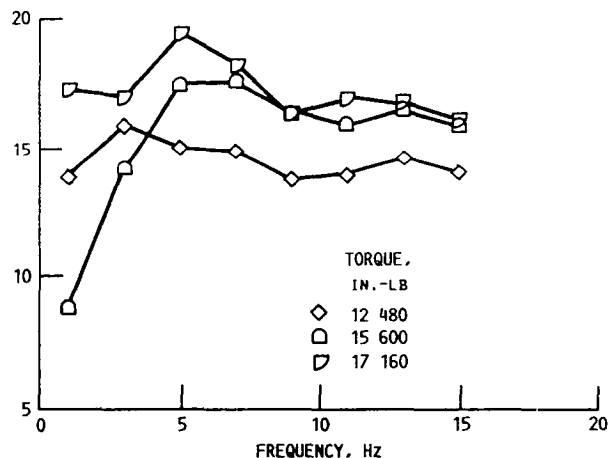
The results of this study will potentially identify axial vibration limits for sprag clutches. This will allow safer and more reliable helicopters to be designed.



(a) SINGLE FORMSPRAG CLUTCH.



(b) DOUBLE FORMSPRAG CLUTCH.



(c) BORG-WARNER CLUTCH.

FIGURE 22. - AXIAL FORCES THAT PRODUCED SLIP AT VARIOUS FREQUENCIES AND LOCKING TORQUES.

**Researchers:** K.C. Radil and A.F. Kascak (AVSCOM) and R.L. Mullen and D. Gasparini (Case Western Reserve).

# Survey of Requirements for Microgravity-Experiment Mechanisms

The development of automated techniques for moving sensitive specimens without exceeding certain acceleration thresholds is critical to successful microgravity experimentation on Space Station Freedom and other future free-flying platforms. To better define these critical acceleration levels and uncover specific requirements for microgravity experiment mechanisms, a survey questionnaire was sent out to over 30 principal investigators working in this field. Responses came from researchers with planned microgravity experiments in the areas of protein crystal growth, solution crystal growth, and directional solidification of alloys, as well as others. Many of the responses indicated the need for advanced mechanism concepts and improved design methodology. There are at least two important reasons for developing advanced microgravity-laboratory mechanisms and robotics. First, automation will ease the demands on the crew's time, which is already limited by the many other tasks they must perform. And second, the crew's interaction with experiments could actually adversely affect the results of some studies by upsetting the microgravity levels.

One survey response identified a need to move a large number (50 to 100) of protein crystal growth cells through a focal plane of a camera, as conceptually illustrated in figure 23. Photomicrographs must be made to record the growth characteristics of the protein crystals as a function of temperature, pH, solution concentration, and humidity. Whether one moves the protein cell carousel or the camera, the maximum disturbance imparted to the specimens can be no larger than  $10^{-6} g/g_0$  (where  $g_0$  is Earth's gravitational acceleration). This acceleration level restriction applies to disturbances on the order of 2 Hz. Above 20 Hz, the specimens are relatively insensitive to disturbances.

This improved protein growth technology will allow researchers to better understand the basic protein building blocks, to tailor

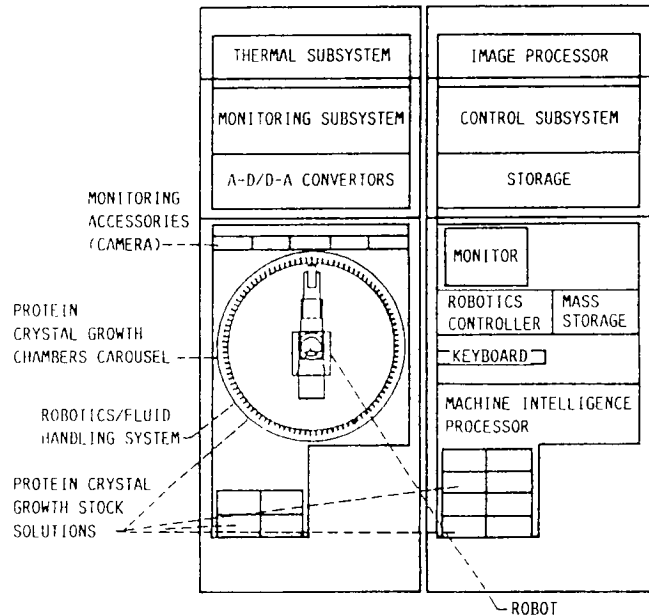


FIGURE 23. - SCHEMATIC OF PROTEIN CRYSTAL GROWTH FACILITY WITH ROBOTIC SERVICER AND PHOTOGRAPHIC RECORDING EQUIPMENT.

crystals for improved cancer treatment drugs, and to improve the state of the art in immunology and tissue transplants.

To meet the technology needs of minimum disturbance laboratory machines, Lewis has begun a program in space mechanisms and robotics. The goals are to identify advanced mechanism, robot joint, and control concepts and to improve laboratory automation design methodology. The mechanism concepts currently under development must meet the difficult design requirements of microgravity experimentation.

---

**Researchers:** B.M. Steinetz and D.A. Rohn (NASA Lewis).

# One-Degree-of-Freedom Reactionless Mechanism

Space Station Freedom and future space platforms will provide the scientific community with expanded microgravity laboratory facilities. Using and maintaining the microgravity environment will require careful attention to the design and development of apparatus for conducting experiments. Since experiments that require microgravity often require physical motion, techniques are required to keep these motions and motion-producing forces from disturbing the experiment or its surroundings. The Reactionless Microgravity Mechanisms and Robotics project is developing precise, smooth, mechanical motion control technology for future space laboratory use.

A single-degree-of-freedom mechanism is being studied as a reactionless (i.e., no net reaction to supporting structure) device. The linear mechanism is representative of devices that will be required to translate a heating element or cooling manifold in an experiment involving rapid quench. An example is the rapid solidification of molten materials, where a sample must be rapidly cooled while it remains in a microgravity environment. Pulling the sample out of a

furnace and placing it in a quenching chamber would obviously place accelerations on it. Instead, the furnace could be quickly moved out of the way and a quenching block put in its place while the sample is motionless. This would require a mechanism that could translate the equipment without allowing undesirable reaction forces to be transmitted into the supporting structure.

The mechanism (fig. 24) is a rotary-to-linear, unlubricated traction drive. Each of the long bars is driven by traction rollers to translate in opposite directions when the motor rotates. One bar represents the mass of the payload, whereas the other is a linear momentum counterbalance. Motor reaction torque and angular momentum are balanced by the motion of the traction ring, which also balances the internal radial loads of the roller drive assembly.

For initial testing, the mechanism was suspended by a cable attached to the base at the center of gravity. All forces and torque couples of interest were in the horizontal plane, so that any uncompensated reactions would show up qualitatively as

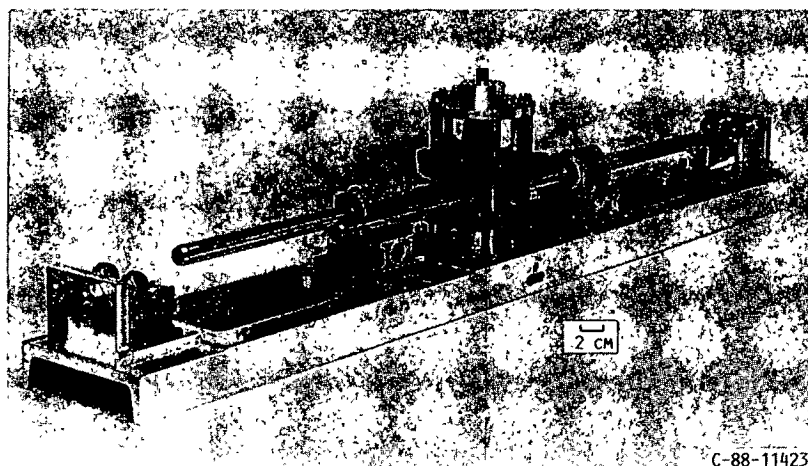


FIGURE 24. - REACTIONLESS, LINEAR ROLLER-DRIVEN MECHANISM.

swinging or swaying motions of the base. Operation showed that the net reaction forces and torques exerted on the base were nearly zero. Deliberate mismatch of bar or ring mass produced visible base motion from the uncompensated reactions.

Plans for further experimentation involve detailed load cell measurements of the effects of mass and momentum imbalance, support bearing friction, traction forces, roller materials, and drive motor character-

istics. Numerical analysis is also underway to model these effects. Technology developed in this proof-of-concept mechanism will be available for designers to incorporate into future prototypes for specific space experiment applications.

---

**Researchers:** D.A. Rohn (NASA Lewis) and J.H. Miller (Sverdrup).

# New Results Concerning the Use of Kinematically Redundant Manipulators in Microgravity Environments

Experimentation and manufacturing in the microgravity environment of Space Station Freedom must be conducted and operated without contaminating the environment with vibrations that disturb the ongoing processes. Robots can be ideal for this work because they are capable of precisely controlled motion. There are two problems associated with material handling in a microgravity environment. The first is transporting specimens without exceeding microgravity accelerations on them. The second is operating the handler without disturbing the microgravity environment with the base reactions or motions of the handler.

The objective of this research is to investigate the feasibility of kinematically redundant robotic manipulators that can perform tasks while maintaining their base reactions below an acceptable level. A manipulator is kinematically redundant if its number of degrees of freedom is greater than that required to accomplish the desired end-effector motion. Its redundant degrees of freedom are used to minimize the cost, which is a weighted sum of the squares of the base reactions.

In the locally optimal trajectory management (LOTM) approach, the cost is minimized at discrete times along the end-effector path. The generalized inverse method is used to solve the inverse kinematics problem. The actual performance of the LOTM approach is not as good as was previously reported. The cost was found to deviate greatly between the minimization points independent of the size of the time steps (figs. 25 and 26). New forms of the Rayleigh-Ritz shape functions are suggested to smooth the joint accelerations. Globally optimal methods (where the cost is the integral over the period of the motion of the weighted square of the base reactions) may prove to be superior. The weights in the cost function should be used as additional parameters in the minimization problem.

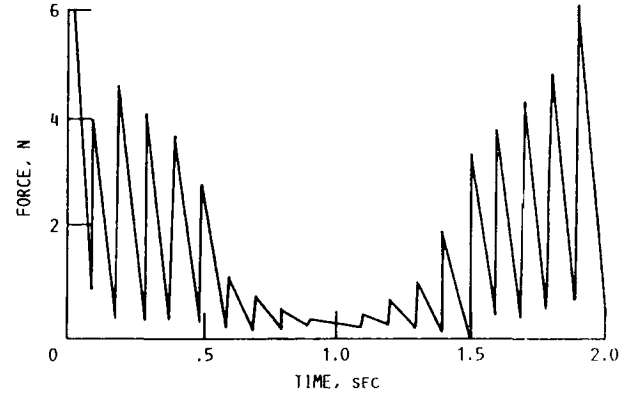


FIGURE 25. - BASE REACTION.

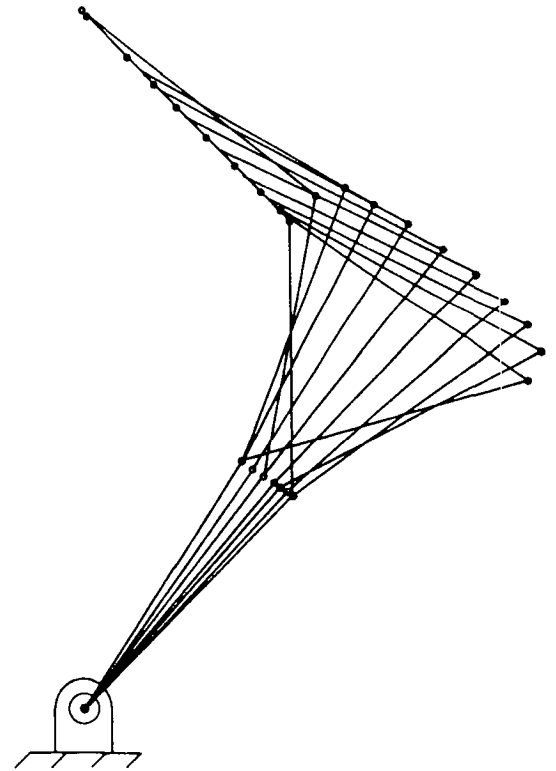


FIGURE 26. - MANIPULATOR.

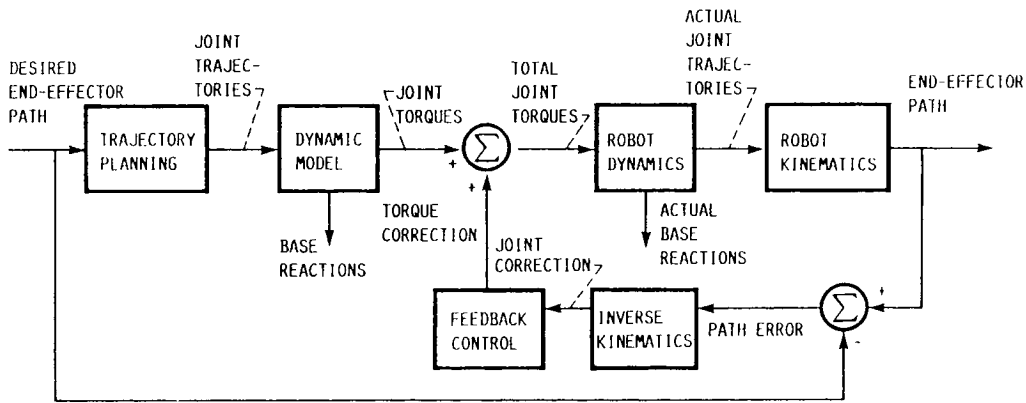


FIGURE 27. - CONTROL STRATEGY.

This two-part control strategy is based on a perturbed dynamic model (fig. 27). Open-loop control torques are computed based on the optimal trajectory management solution and on the zero-order equations of motion of the manipulator. The closed-loop controller is based on the first-order perturbed dynamic model; it corrects joint motion errors observed in dynamic simulations. The joint motion error is the difference between the actual joint motion and the optimal joint motion. The feedback controller effectively applies active springs and dampers at the joints causing the rigid-

linked manipulator to act as a flexible structure. The control gains are chosen to be proportional to the diagonal elements of the inertia matrix to conform to uniform damping control. The effects of the closed-loop control on the base reactions are relatively small.

---

**Researchers:** R.D. Quinn and N.J. Lin (Case Western Reserve) and C. Lawrence (NASA Lewis).

# A Global Approach for Using Kinematic Redundancy to Minimize Base Reactions of Manipulators Used in Microgravity Environments

In the near future, autonomous robotic manipulators will be used on space stations to perform exhaustive tasks such as repairing the station's exterior and performing delicate experiments under microgravity conditions. Such manipulators will, in general, have redundant degrees of freedom in order to perform tasks. (It is well known that redundant manipulators can be used to avoid obstacles and singular configurations.)

An issue of considerable importance for manipulators used in microgravity environments is the minimization of the magnitudes of the dynamic reaction forces and moments exerted by the manipulator on its base as it performs its task. Furthermore, the base reactions of these manipulators should be minimized or eliminated so that their base forces and moments do not disturb other tasks or experiments in the vicinity.

A local approach to this problem was previously described and implemented. However, the local approach led to undesirable peaks in the base reactions at certain instants of time. To smooth out these undesirable peaks, a global approach that uses an integral performance index over the entire end-effector trajectory was implemented and a performance index, or cost function, was minimized at each point of the end-effector trajectory in order to determine the joint-space trajectories.

The basic rationale which underlies the global approach is as follows. Planning a trajectory for a manipulator reduces to the problem of solving the inverse-kinematic problem for the joint-variables, or joint-space, trajectory given the specified trajectory in the task space. In the case of a (kinematically) redundant manipulator, the inverse-kinematic problem has an infinite number of solutions. An optimization problem of minimizing the base reactions was posed to obtain a unique solution to the inverse-kinematic problem: in this way the redundant degrees of freedom were used to obtain joint-space trajectories that

minimize base reactions. In the present research, an integral performance index (which is a function of the reaction forces and moments exerted on the base) is minimized.

To minimize the base reactions, the joint trajectories must be smooth. In addition, the angular velocity and acceleration at both the initial and end points of the joint trajectory should be zero. High-order polynomials (or splines) can represent this family of curves by satisfying the velocity and acceleration boundary conditions. Since very high order polynomials behave unpredictably, the joint trajectory is often broken into a number of segments which can be represented by lower-order polynomials, such as third and fourth order. These segments satisfy the boundary conditions and are continuous from one segment to another. In this research, a three-segment method was considered. It consists of initial, transitional, and final segments. Two fourth-order polynomials are used for the initial and final segments, and a third-order polynomial is used for the transitional segment. This method is also known as the 4-3-4 joint trajectory representation. The curves described by this method are functions of the initial and final joint positions, the time period of the transitional segment, and the distance traversed during the transitional period.

For a redundant manipulator with  $(m-n)$  degrees of redundancy, applying the three parameters scheme to the redundant joint variables, there are  $3(m-n)$  independent variables. To determine the optimal values for vectors  $\alpha$ ,  $\beta$ , and  $\theta_f$ , a performance index or cost function is used as a criterion. The present approach solves the joint variables by posing the minimization of the base reactions problem as an optimization problem.

---

**Researchers:** C.L. Chung and S. Desa (Carnegie-Mellon University) and C. Lawrence (NASA Lewis).

# Characterization of Structural Connections by Using Free and Forced Response Test Data

The need for parameter identification methods to improve structural dynamic models has been increasing. The ability of engineers to construct complex analytical models has increased; however, they are still unable to adequately simulate observed response with those models. Although great strides in computer technology and analytical methods have enabled engineers to solve very large and complex structural problems theoretically, the results often do not compare well with test data because of inaccuracies in the parameters of the mathematical model.

Parameter identification methods may be used to determine structural connection properties. Since connections usually contribute significantly to the overall system stiffness, damping, and in many cases nonlinearity, it is critical that reliable connection models be made available. For many structural systems, the constituent components often can be modeled accurately: the connections contain most of the modeling uncertainty. Therefore, accurate system response predictions often are highly dependent on valid connection models.

In the present research, parameter identification methods are extended so that they can be used for the identification of linear as well as nonlinear connection parameters. The present procedure is suitable for processing test data that have been measured at arbitrary stations on the structural system. The data need not be measured directly at the connection boundaries. This flexibility is highly desirable because in most practical situations it is impossible to obtain test data at the connection boundaries, and other identification methods are ineffective.

The procedure requires verified analytical models of the individual components, although the connection parameters to be identified may be nonlinear, and velocity or displacement dependent. Adequate, transient time-domain response data are required for the assembled structural system; the location of data measurement stations is, however,

arbitrary. Limited measurement errors in the data may be accommodated through an iterative refinement process in the identification algorithm (fig. 28). The quality of the parameter identification is dependent on the quantity as well as the quality of the system transient response data available.

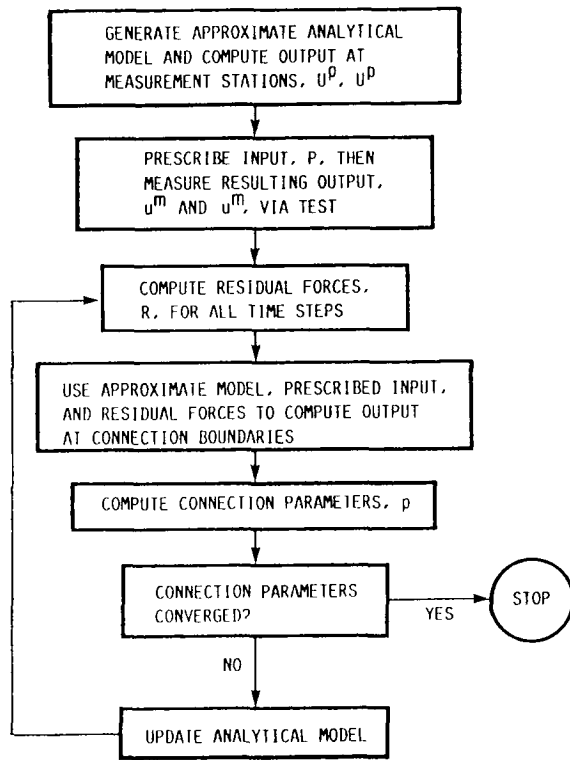


FIGURE 28. - IDENTIFICATION PROCEDURE.

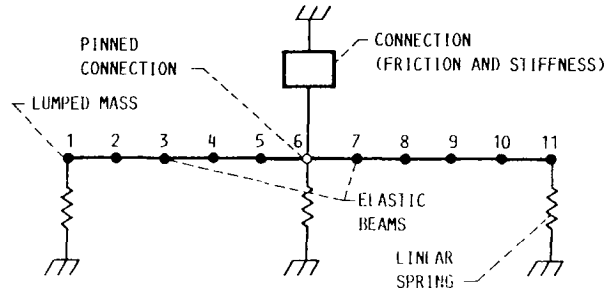
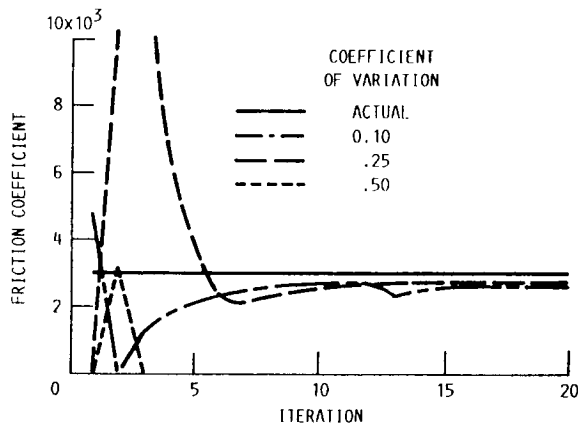
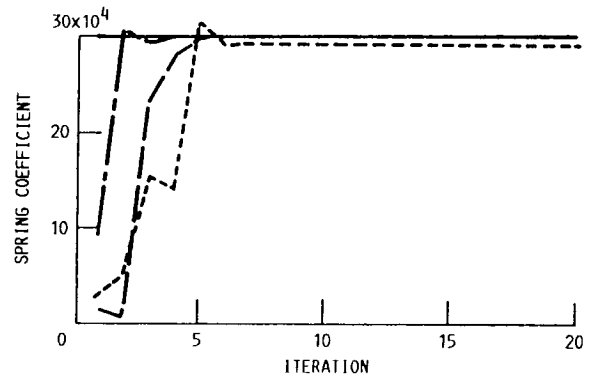


FIGURE 29. - STRUCTURAL DYNAMIC SYSTEM.



(a) FRICTION.



(b) LINEAR SPRING.

FIGURE 30. - IDENTIFIED PARAMETERS FOR MODEL WITH FRICTION DAMPING AND SPRING STIFFNESS.

The number of parameters to be identified is not limited, although larger identification problems may require a greater number of measurement stations. The procedure shows great promise for improving modeling capabilities in complex structural systems, as well as for enhancing our understanding of structural connection behavior (figs. 29 and 30). Further developments are certainly desirable in establishing convergence criteria, enhancing convergence, determining the

reliability of identified parameters, characterizing more complex connections, and streamlining the identification of large problems.

---

**Researchers:** C. Lawrence (NASA Lewis) and A.A. Huckelbridge (Case Western Reserve).

# Distributed Finite Element Analysis Using a Transputer Network

ORIGINAL PAGE

BLACK AND WHITE PHOTOGRAPH

Finite element analysis is used extensively in evaluating the load and life capabilities of structures from small to large and simple to complex. Complex structures with thousands of independent degrees of freedom, typically, are analyzed by using expensive supercomputers for reasonable computation times. However, the performance of supercomputers can be approached and even exceeded with parallel processing networks that use low-cost processors.

Under a Small Business Innovation Research contract to the NASA Lewis Research Center, Sparta, Inc., developed a desktop-sized parallel processing workstation capable of supercomputer performance. The workstation (fig. 31) consists of a network of 32 interconnected transputers operated from an IBM PC-AT compatible host computer. It also has a large-screen color graphics system used for interactive processing and postprocessing. Two 100-MB (megabyte) disk drives provide a mass storage system for the network.

The INMOS T800 transputers used in the workstation are powerful computers with processors, memory, and communication capability contained on a single 1-in.<sup>2</sup> chip. Each transputer has four two-way communication links that can be connected to other transputers in a wide variety of network architectures. This workstation network is configured as two interconnected 16-processor tetrahedra, as shown in figure 32.

A distributed finite analysis method was implemented on the workstation. Preprocessing tasks for two-dimensional models include problem definition, geometric modeling, and mesh generation. An adaptive analysis based on Quadtree theory was implemented for two-dimensional models. Three-dimensional models are input via a NASTRAN interface. With 1 MB of memory available to each processor, the two- and three-dimensional solvers can handle up to 20 000 degrees of freedom.

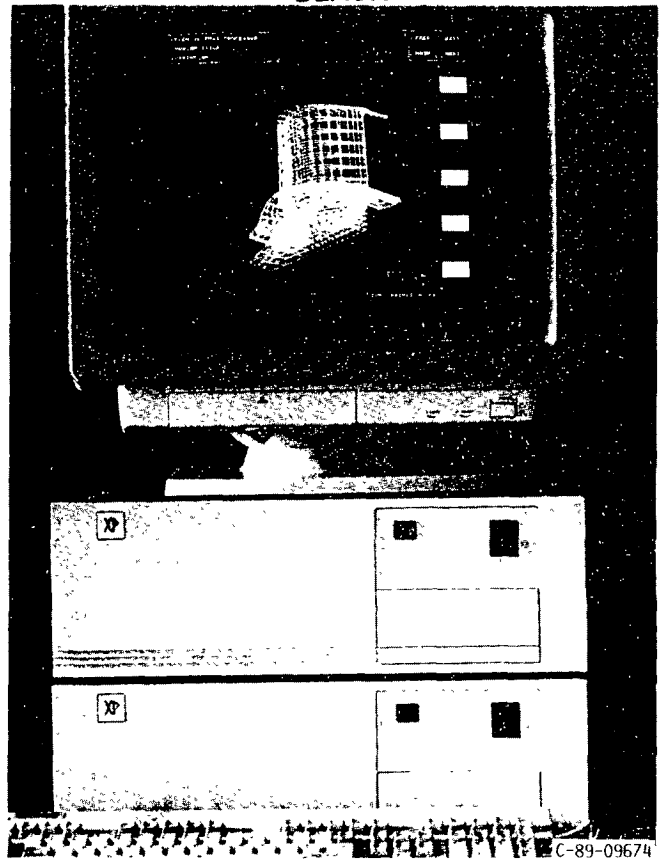


FIGURE 31. - TRANSPUTER-BASED FINITE ELEMENT ANALYSIS WORKSTATION.

Postprocessing gives a display of the deflections. Stress contours can be displayed for two-dimensional models.

A space shuttle main engine turbine blade model was used to demonstrate the capability of the workstation. The blade model had about 1500 nodes and 4500 independent degrees of freedom. The workstation executed the analysis at about one third the speed of a CRAY X-MP24. This gives the workstation a cost-performance ratio about 60 times better than a CRAY X-MP24 system.

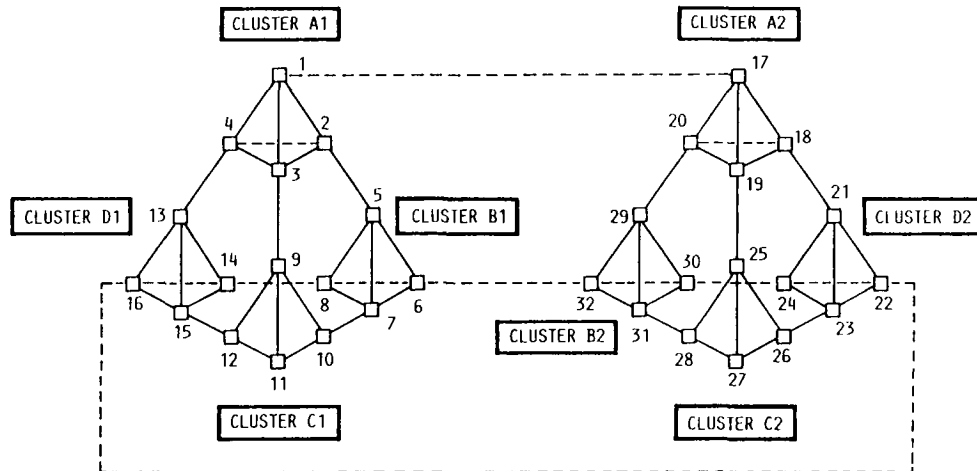


FIGURE 32. - TRANSPUTER NETWORK COMMUNICATION CONFIGURATION.

**Researchers:** J.W. Watson (Sparta) and D.C. Janetzke and L.J. Kiraly (NASA Lewis).

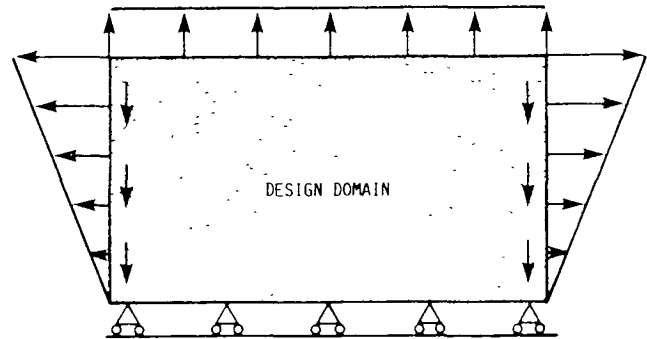
# Shape and Topology Optimization by the Homogenization Method

A major difficulty in optimizing the shape of linearly elastic structures is caused by large domain changes during the optimization process which require the domain to be discretized for the finite element stress analysis. Furthermore, changes of topology, such as the introduction of weight-saving holes in the structure, are virtually impossible with existing optimization approaches, unless they are done manually. A new method is under development to overcome the limitations of traditional shape optimization. Optimization and discretization are performed in a fixed domain by using a unit-cell approach to automatically generate the optimal shape and topology from a fixed domain under given loading and support conditions. The design is identified with the parameters of (1) shape and (2) relative size of voids for the unit cells. The shape optimization problem is transformed into a void distribution problem, and the optimal design corresponds to the best distribution of the unit-cell properties.

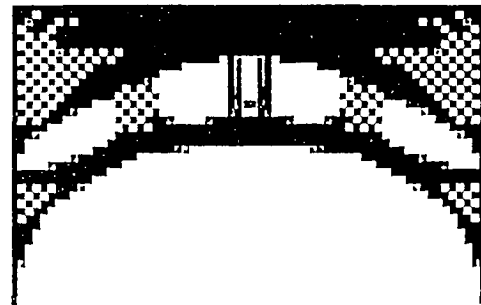
The design domain is discretized into a gridwork pattern with the unit-cell volumes initially full. The design boundary and internal topology are modified sequentially until the structural compliance is minimized for a user-defined allowable structural weight (i.e., volume  $\times$  density). Currently the program warns the user if a limit on a unit stress measure, such as von Mises stress, is exceeded. It is planned to implement an optimality criterion to minimize the maximum value of a local stress measure in the body such as von Mises stress, subject to an isoparametric constraint on structural weight.

Numerical results have been obtained for several problems including a general structure with load and boundary conditions, as shown in figure 33(a). In this problem the design goal was to optimize the structure's design boundary and topology for two prescribed final weights. The converged

structural designs weighing only 38 and 25 percent of the original design are shown in figure 33, parts (b) and (c), respectively. As shown by the current results, the numerical approach can easily accommodate large



(a) DESIGN DOMAIN WITH PRESCRIBED LOAD AND BOUNDARY CONDITIONS. ALL UNIT-CELL VOLUMES ARE FULL.



(b) FINAL DESIGN: 38 PERCENT OF INITIAL WEIGHT.



(c) FINAL DESIGN: 25 PERCENT OF INITIAL WEIGHT.

FIGURE 33. - APPLICATION OF THE UNIT-CELL OPTIMIZATION METHOD TO TWO-DIMENSIONAL, LINEARLY ELASTIC STRUCTURE WITH TWO STRUCTURALLY-EFFICIENT, LIGHTWEIGHT FINAL DESIGNS.

movements of the design boundary and automatically introduce weight-saving cutouts in lightly loaded areas.

The numerical approach can also be used to analyze composite material structures. Modeling the matrix and fibers with unit-cells having appropriate stiffness properties,

the macroscale elastic constants are determined by using the homogenization method.

---

**Researchers:** N. Kikuchi and J. Taylor  
(University of Michigan) and B.M. Steinetz  
(NASA Lewis).

# Parallel Time Integration of Finite Element Problems

In this study, a system of transputer computers was used to solve structural dynamics problems. A transputer is a chip-level computer with local memory and four asynchronous communication channels that can be linked to other transputers. The transputers can be arranged in a variety of configurations; however, each transputer can have at most four neighbors. In this study a pipeline configuration was used. The transputers were programmed using the OCCAM language, which simplifies the programming of parallel algorithms.

The central difference rule (a direct time integration method) was used to solve the governing structural dynamics equations. With direct integration methods the time period of interest is divided into intervals or steps, and the solution is progressively computed at each of these time steps. The central difference method is said to be an explicit method since it does not require the solution of algebraic equations. Therefore, the displacement at a node can be computed independently of the other nodes. For parallel processing, the nodes of the mesh are partitioned into groups. These groups are assigned to different processors for updating, and information is exchanged between processors after each update. In this study, only nearest-neighbor communication was necessary.

The test problem chosen for study was a two-dimensional plate that was fixed at one end and had an applied load at the other end (fig. 34). The size and geometry of the problem was varied by changing the number of nodes in the x and y directions. For example, the notation 20 x 10 indicates that the plate was divided into 20 nodes in the x-direction (nnodex = 20) and 10 nodes in the y-direction (nnodey = 10). In this case the total number of nodes would be 200 (nnodex x nnodey). The three-node triangle finite element was used in this study. The problem was partitioned for parallel processing by dividing the domain into subdomains with vertical lines; then the nodes in each subdomain were assigned to a processor (fig. 34). In all cases an equal number of nodes were assigned to each processor.

The results for the first series of test problems for various numbers of time steps are given in table I. Two processors were used for problems with 100, 200, and 400 nodes. It can be seen from the data that, once a sufficient number of time steps were run to overcome the overhead involved in setting up the problem to run in parallel, the solution time was proportional to the size of the problem.

In the second series of problems, size was varied so that the number of nodes per processor was fixed at 50 and the number of processors was varied from two to eight. Note that the eight-processor problem is four times as large as the two-processor problem. When only one processor is used, the solution of a 50-node problem takes 31.7 sec for one-thousand time steps. If the parallel algorithm were perfectly efficient, the solution times for the three cases would be equal to the one-processor solution time. From table II it is evident that some efficiency is lost because of insufficient interprocessor communication. However, it appears that for the one-thousand time step case additional processors could be used, thereby increasing the problem size, with little increase in the solution time.

The third series of problems investigated how the solution time varied as the amount of interprocessor communication was

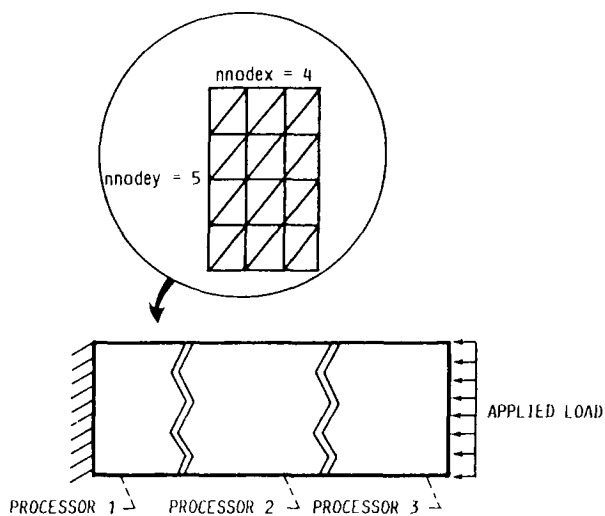


FIGURE 34. - PROBLEM STATEMENT FOR FINITE ELEMENT TEST PROBLEM.

TABLE I. - SOLUTION TIMES FOR VARIOUS SIZE PROBLEMS  
USING TWO PROCESSORS

Number of time steps	Time, sec		
	10 by 10 nodes	20 by 10 nodes	40 by 10 nodes
1	0.3	1.0	1.8
10	.6	1.7	5.0
100	4.0	8.4	18.5
1000	37.4	75.2	153.5

TABLE II. - SOLUTION TIME FOR VARIOUS NUMBERS OF PROCESSORS WHERE THE NUMBER OF NODES PER PROCESSOR IS FIXED

Number of time steps	Time, sec		
	Two processors; 10 by 10 nodes	Four processors; 20 by 10 nodes	Eight processors; 40 by 10 nodes
1	0.30	0.58	1.02
10	.64	.99	1.43
100	3.98	5.06	5.50
1000	37.44	45.78	46.29

TABLE III. - SOLUTION TIMES USING EIGHT PROCESSORS FOR PROBLEMS WITH DIFFERENT NUMBERS OF NODES IN THE X AND Y DIRECTIONS

Number of time steps	Time, sec			
	80 by 10 nodes	40 by 20 nodes	20 by 40 nodes	10 by 80 nodes
1	3.28	3.83	4.96	7.54
10	4.02	4.68	5.99	8.92
100	11.44	13.23	16.33	22.69
1000	85.64	98.73	119.71	160.37

increased. The number of nodes per processor was fixed at 100 while the lengths of the problem in the x- and y-directions were varied. Since the problems were partitioned by vertical lines, the interprocessor communication was proportional to the number of nodes along the interface in the y-direction. For example, the 80 by 10 problem has 10 nodes along the interface. As shown in table III, the solution time increases with increasing amounts of interprocessor communication.

This study shows that the transputer can be used to solve complex structural dynamics problems and that the best performance is obtained when the processor computation-to-communication ratio is large.

However, some issues require further investigation:

- (1) Given the geometry of the problem, how can the processors be arranged and the problem partitioned to minimize interprocessor communication?
- (2) Can non-nearest neighbor communication be used without a substantial loss in efficiency?

---

**Researchers:** P.J. Smolinski (ICOMP) and D.C. Janetzke and L.J. Kiraly (NASA Lewis).

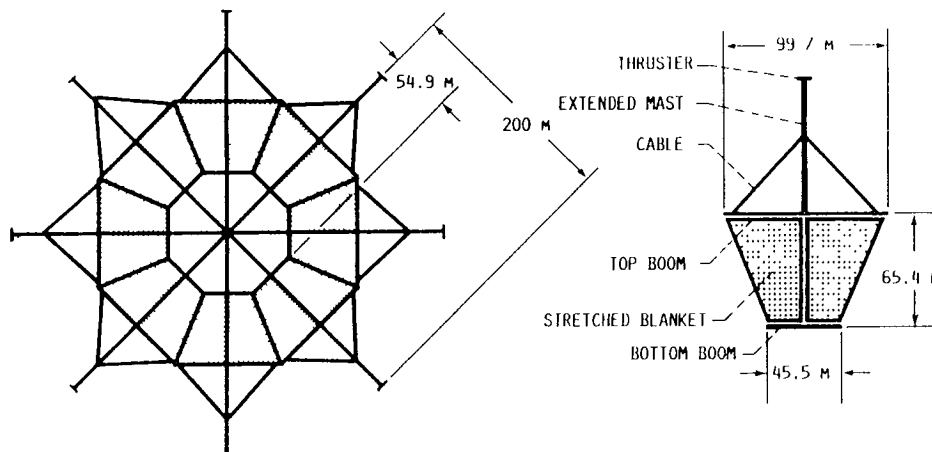
# Structural Design of a 6-MW Solar Electric Propulsion (SEP) Spacecraft for Mission to Mars

A preliminary estimate of the structural configuration and mass for the proposed Solar Electric Propulsion (SEP) Mars Spacecraft recently was completed. The design is based on a 6.32-MW initial power specification and an array area of 38 028 m<sup>2</sup>. The payload and thruster masses were specified as 400 000 and 115 000 kg, respectively.

The proposed configuration shown in figure 35 would accommodate these solar array area and thruster dimensional requirements. The array system was made octagonal because the requirement for eight thrusters will necessitate the use of eight structural masts to transfer the thruster loads into the spacecraft. Furthermore, the octagonal shape maximizes the area available for the solar arrays, maintains symmetry (duplicate arrays), and provides a logical structural framework (split blanket arrays). The dimensions of the configuration were determined from the specified array area of 38 028 m<sup>2</sup>, the payload area of 10 000 m<sup>2</sup>, and the thruster extension of 200 m. Eight individual arrays, each having independent pointing capability, will be required.

Table IV compares three proposed solar-powered spacecraft: Space Station Freedom, TRW's Advanced Photovoltaic Solar Array (APSA), and the present SEP spacecraft. Although Space Station Freedom and APSA have power and mission requirements that differ significantly from the SEP, they provide a reasonable basis for extrapolating design parameters for the SEP. Using the specific power (W/kg) of the APSA as a starting point and considering the significant increase of array size of the SEP (weight per area usually decreases with size) yields the projection that the SEP design may attain a specific power of at least 150 W/kg. This value probably is conservative considering TRW's projection of 300 W/kg for future solar-powered spacecraft. (Advanced Photovoltaic Solar Array Design, Contract NAS7-918, TRW Space and Technology Group, November 1986). The total array weight associated with 150 W/kg and 6.3 MW is 42 000 kg.

The octagonal configuration lends itself to the two-wing center mast designs which were used for both the Space Station Freedom and APSA designs. However, the



(a) 38 000 m<sup>2</sup> CONFIGURATION.

(b) SPLIT BLANKET SOLAR ARRAY (EIGHT REQUIRED).

FIGURE 35. - 6.32-MW SOLAR ELECTRIC PROPULSION SPACECRAFT.

TABLE IV. - SOLAR ARRAY COMPARISONS

Solar array	Power	Number of arrays	Total area of arrays		Total array weight		Specific power, W/kg	Power density, W/m <sup>2</sup>	Stiffness, Hz
			m <sup>2</sup>	ft <sup>2</sup>	kg	lb			
Space Station Freedom (low-earth orbit)	75 kW	8	2400	25 800	6080	13 300	12	31	0.10
TRW Advanced Photovoltaic Solar Array (geosynchronous orbit; gallium arsenide)	10 kW	2	85	910	76	168	136	134	.10
Solar Electric Propulsion Mars Spacecraft (interplanetary)	6.3 MW	8	38 028	400 000	<sup>a</sup> 42 000	90 000	<sup>b</sup> 150	166	<sup>c</sup> <.10

<sup>a</sup>Boom extension not included.

<sup>b</sup>Assumed specific power.

<sup>c</sup>Projected value.

SEP is much larger than these other solar designs, and the top cross member on the SEP is longer than the bottom cross member (nonrectangular blankets). Neither of these differences should present complications although the design of the cross members and boom probably will differ because of the large dimensional dissimilarities in relation to the previous designs (e.g., continuous beams for the APSA vs. post-tensioned truss structures for the SEP).

It is not yet clear exactly how the structural components will look, but it is expected that the mast and boom cross-sectional areas will increase and the other components may remain relatively unchanged

in comparison to the smaller spacecraft. The overall design most likely will be constrained by a lower stiffness limit (e.g., 0.1 Hz) and a demand to withstand a maximum acceleration level (e.g., 0.01 g). Because of the large size of this structure, post-tensioned guide wires might be used to provide stiffness and a means for suppressing vibration. Cables might also be used to minimize the blanket substrate thickness (and weight) by relieving the substrate from having to carry all of the blanket tension loading.

**Researchers:** C. Lawrence and E.H. Meyn (NASA Lewis).

# Solution and Sensitivity Analysis of a Complex Transcendental Eigenproblem With Pairs of Real Eigenvalues

Dynamic stability analysis of aeroelastic systems consists of finding the real values of Mach number  $M$  and vibration frequency that satisfy the following equations of motion:

$$[-\omega^2 M + K - C_1(M, \omega)]q = 0$$

where  $M$ ,  $K$ , and  $C$  are the generalized mass, stiffness, and aerodynamic matrices, respectively. The aerodynamic matrix is a transcendental function of  $M$  and  $\omega$ . These equations can be viewed as defining a complex transcendental eigenvalue problem of the form  $A(\lambda_1, \lambda_2)u = 0$  with pairs of real eigenvalues defined by  $\lambda_1$  and  $\lambda_2$  and with eigenvectors defined by  $u$ .

This eigenvalue problem differs in many respects from the conventional linear eigenvalue problem defined by  $(A - \lambda I)u = 0$  and the  $\lambda$ -matrix eigenvalue problem defined by  $A(\lambda)u = 0$ . Whereas the linear and the  $\lambda$ -matrix eigenproblems define eigenpairs, the eigenvalue problem we consider defines eigentriples. Also, it is well known that, when multiplicity is properly accounted for, the number of eigenpairs of the linear eigenvalue problem depends only on the order of the matrix and, in the case of the  $\lambda$ -matrix eigenproblem, on the matrix order and the highest degree of the polynomials in  $\lambda$ . In the case of the transcendental eigenvalue problem, the number of the eigentriples is not known in advance and could be infinite, finite, or none. In addition, no orthogonality relationships or canonical forms are known to exist for the transcendental eigenvalue problem with pairs of real eigenvalues.

In this study, the condition of a vanishing determinant for the existence of a nonzero vector  $u$  is used to obtain the values of  $\lambda_1$  and  $\lambda_2$ . The eigenvector  $u$  is obtained afterwards by inverse iteration. It is first shown that all the derivatives of the determinant can be evaluated at the cost of a single matrix inversion. The previously experienced

problem of slow convergence is alleviated by developing a new quasi-Newton method, based on Broyden's updates for the derivatives of the matrix  $A$ . A practical iterative scheme for solving the determinant equation with a convergence rate approaching that of the quadratically convergent Newton's method is proposed. Newton's method, however, cannot be used in most applications because it is impractical to compute the analytical derivatives of the aerodynamic matrix. Tables V and VI show, for two examples, the number of iterations required for convergence starting with various initial guesses. The tables demonstrate that the present procedure is far superior to Broyden's method in terms of the number of iterations required for convergence. Comparison to Newton's method also demonstrates that at most two more iterations are required with the present procedure than with Newton's method. Thus, the present solution procedure appears to have a rate of convergence that is close to that of Newton's method.

TABLE V. - COMPARISON OF RATE OF CONVERGENCE - EXAMPLE 1  
[Eigenpair of interest is  $\lambda_1 = 0.5$  and  $\lambda_2 = 1.5$ .]

Initial guess of eigenvalues		Number of iterations for convergence		
$\lambda_1$	$\lambda_2$	Newton's method	Present method	Broyden's method
0.4	1.5	3	4	4
.7	1.5	3	4	6
.3	1.3	3	5	6
.3	1.7	3	5	6
.7	1.3	3	5	6
.7	1.7	3	5	6
.9	1.9	4	6	10
.9	1.1	4	6	10
.4	1.9	4	5	13
.4	1.1	4	5	13

TABLE VI. - COMPARISON OF RATE OF CONVERGENCE - EXAMPLE 2

[Eigenpair of interest is  $\lambda_1 = 0.5$  and  $\lambda_2 = 0.1$ .]

Initial guess of eigenvalues		Number of iterations for convergence		
$\lambda_1$	$\lambda_2$	Newton's method	Present method	Broyden's method
0.51	0.11	5	5	19
.54	.14	9	10	No convergence
.60	.20	14	20	No convergence
.58	.09	6	6	21
.49	.11	5	5	14
.49	.12	6	6	38
.48	.11	4	4	8

Optimization of aeroelastic systems also requires efficient computation of the derivatives of the eigenvalues and eigenvectors with respect to design variables. The computation of these derivatives is referred to as sensitivity analysis. Two computational algorithms are presented for calculating the sensitivities of the eigenvalues and the corresponding eigenvectors with respect to design parameters.

The first algorithm computes the sensitivities of the eigenvalues only and requires the computation of the left eigenvectors. The second algorithm computes the sensitivities of the eigenvalues as well as the eigenvectors in an integrated manner. This algorithm requires the solution of a system

of linear equations of about the same order as the matrix in the eigenproblem. The left eigenvectors are not required in this approach. However, the information contained in the left eigenvectors may be used to assure that this system of linear equations is optimally conditioned. The algorithms presented are verified by applying them to the example problems.

These algorithms are expected to prove useful in aeroelastic sensitivity analysis and optimization procedures.

---

**Researchers:** D.V. Murthy (University of Toledo) and G.L. Stefko (NASA Lewis).

# Nonlinear Unsteady Supersonic Axial Flow Aerodynamics

Previous experimental research on the supersonic throughflow fan (SSTF) concept is extremely limited. Therefore, to evaluate the concept and potential of an SSTF, NASA Lewis is currently conducting a research effort to design, build, and test an SSTF. During the original design of the rotor blades, aeroelastic stability became a concern. Consequently, a linear, two-dimensional unsteady potential theory presented by Lane for cascades with supersonic leading-edge locus was developed into a computer program and incorporated into an existing aeroelastic code for use in the aeroelastic stability analysis of the SSTF.

To improve analytical aeroelastic analysis capabilities, Lewis desired to incorporate the effects of thickness and camber into its aeroelastic model. Therefore, Lighthill's nonlinear piston theory was used as a first attempt to include thickness and camber effects in an analytical aeroelastic analysis for cascades with supersonic leading-edge locus. As a result, the existing unsteady aerodynamic code using Lane's linear potential theory was modified to include the nonlinear piston theory.

As shown in figure 36, nonlinear effects are included in the calculation of the

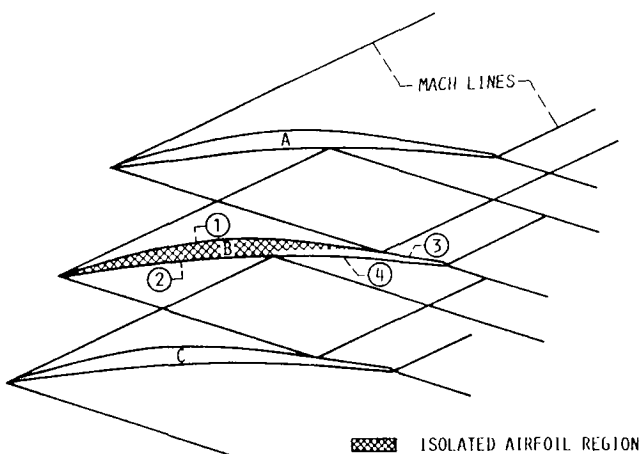


FIGURE 36. - CASCADE IN SUPERSONIC AXIAL FLOW. SURFACES (1) AND (2) EXHIBIT ISOLATED AIRFOIL BEHAVIOR. LIGHTHILL'S PISTON THEORY IS USED TO CALCULATE UNSTEADY PRESSURES ON SURFACES (1) AND (2), AND LANE'S LINEAR POTENTIAL THEORY IS USED TO CALCULATE UNSTEADY PRESSURES ON SURFACES (3) AND (4)



FIGURE 37. - SUPERSONIC THROUGHFLOW FAN AIRFOIL PROFILE.

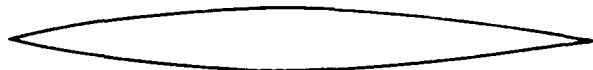


FIGURE 38. - SUPERSONIC THROUGHFLOW FAN THICKNESS (SYMMETRIC PROFILE) DISTRIBUTION.

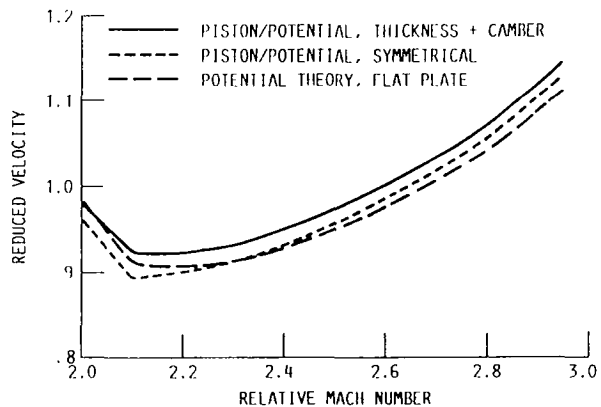


FIGURE 39. - TORSIONAL MODE FLUTTER BOUNDARY FOR THE SUPERSONIC THROUGHFLOW FAN.

unsteady pressures in the isolated airfoil regions by using nonlinear piston theory. The unsteady pressure on the remaining airfoil surfaces are calculated with Lane's linear potential theory.

The original SSTF airfoil profile (thickness and camber) and the symmetric profile (thickness distribution only) are shown in figures 37 and 38, respectively. An aeroelastic stability analysis was performed on the SSTF cascade by using the original airfoil geometry (fig. 37) as well as the symmetric profile (fig. 38) in conjunction with nonlinear piston theory. These results were compared with results from the potential theory for flat plates. The resulting flutter instability boundaries for the SSTF cascade are presented in figure 39.

The analysis with the symmetric profile (thickness distribution only) decreased the stability of the SSTF cascade for  $2 < M < 2.3$  and increased the stability at Mach numbers above 2.3 when compared with an analysis using linear potential theory on flat plates. The inclusion of the original airfoil geometry increased the predicted stability for Mach numbers slightly above 2 with respect to the analysis using linear potential theory on

flat plates. The inclusion of camber with thickness (original airfoil geometry) also increased the stability of the SSTF cascade when compared with the analysis with thickness only (symmetric profile).

---

**Researcher:** J.K. Ramsey (NASA Lewis).

# Numerical Analysis of Supersonic Flow Through Oscillating Cascade Sections by Using a Deforming Grid

To evaluate the concept and potential of a supersonic throughflow fan (SSTF), NASA Lewis is currently conducting a research effort to design, build, and test an SSTF. Understanding the aeroelastic behavior and identifying flutter boundaries are critical in such new designs. Many existing aerodynamic flutter analysis methods are based on linear flat plate theory, which only approximates the blade thickness and camber. One alternative is to use a finite difference algorithm to predict the flowfield and account for these effects.

A finite difference code based on Euler equations was developed to analyze the supersonic throughflow fan. The three-dimensional fan is modeled as a two-dimensional cascade of airfoils in supersonic axial flow. Harmonic pitching motions are prescribed for the blade sections for both zero and nonzero interblade phase angles  $\sigma$  (i.e., for blade motions in phase with each other and blade motions differing by a constant phase angle between the adjacent blades). A deforming grid technique is used to specify the periodic boundary conditions during oscillation.

Figures 40 to 42 show some of the results obtained with the present code. The results were obtained for a Mach number  $M$  of 2.61, a stagger angle  $\gamma$  of  $28^\circ$ , a gap to chord ratio  $g/c$  of 0.311, and a reduced frequency based on semichord  $k$  of 0.5.

Figure 40 compares the unsteady pressure from a linearized (Lane's) theory and the present finite difference solution for a flat plate cascade for a  $180^\circ$  interblade phase angle. A thickness ratio of 0.005 is assumed for the flat plate. The results are obtained for a zero steady-state angle of attack. The agreement with Lane's theory is good for both the real and imaginary parts of pressure, except that the locations of the shock reflections were predicted about 10 percent forward of the Lane's theory predictions. The finite thickness approximation of the flat plate used in the Euler code is suspected of contributing to this error. The wiggles near the leading edge of the Euler solution are numerical and are reduced for real airfoils. The force coefficients obtained by integrating these pressures are insensitive to these wiggles.

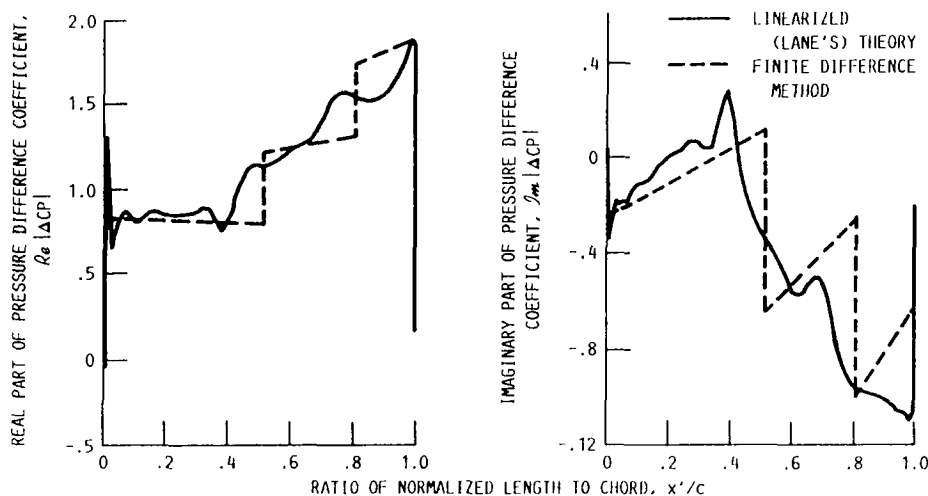


FIGURE 40. - FIRST HARMONIC PRESSURE DIFFERENCE DISTRIBUTION FOR FLAT PLATE CASCADE. STAGGER ANGLE,  $\gamma$ ,  $28^\circ$ ; GAP-TO-CHORD RATIO,  $g/c$ , 0.311; INLET FLOW ANGLE,  $\beta_1$ ,  $28^\circ \pm 0.10^\circ$ ; REDUCED FREQUENCY BASED ON SEMICHORD,  $k$ , 0.5; INTERBLADE PHASE ANGLE,  $\sigma$ ,  $180^\circ$ .

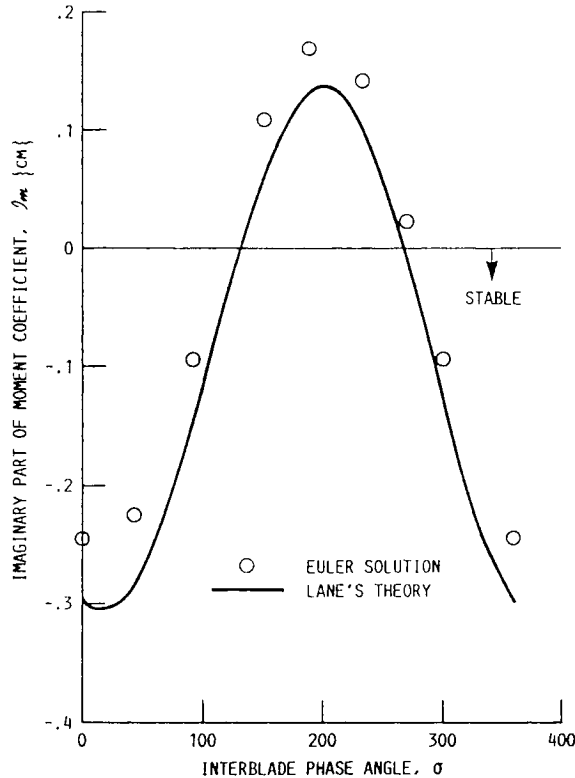


FIGURE 41. - IMAGINARY PART OF MOMENT COEFFICIENT VERSUS INTERBLADE PHASE ANGLE: FLAT PLATE CASCADE. INLET MACH NUMBER,  $M_1$ , 2.61; STAGGER ANGLE,  $\gamma$ , 28; GAP-TO-CHORD RATIO,  $g/c$ , 0.311; INLET FLOW ANGLE,  $\beta_1$ ,  $28^\circ \pm 0.10^\circ$ ; REDUCED FREQUENCY BASED ON SEMI-CHORD,  $k$ , 0.5.

Figure 41 shows the variation of the imaginary component of the moment coefficient with interblade phase angle for the flat plate cascade. When the imaginary part of the moment coefficient becomes positive, the moment leads the motion of the flat plate and represents an unstable condition. The predictions for Lane's theory are also shown in figure 41. The agreement is very good over all interblade phase angles in spite of the different shock locations.

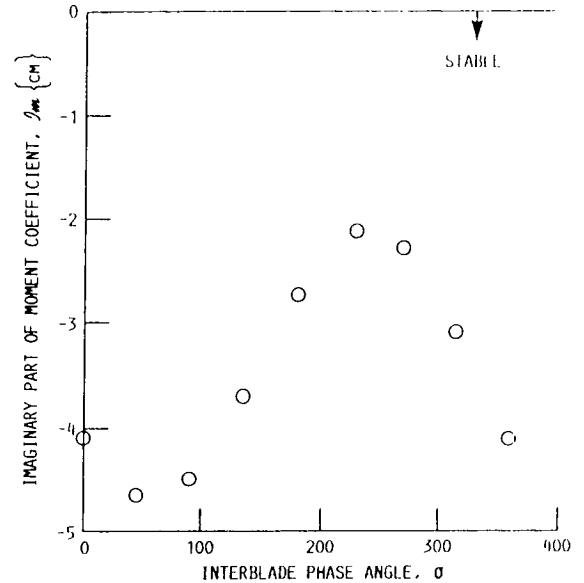


FIGURE 42. - IMAGINARY PART OF MOMENT COEFFICIENT NEAR MIDCHORD VERSUS INTERBLADE PHASE ANGLE: ROTOR CASCADE. INLET MACH NUMBER,  $M_1$ , 2.61; STAGGER ANGLE,  $\gamma$ , 28; GAP-TO-CHORD RATIO,  $g/c$ , 0.311; INLET FLOW ANGLE,  $\beta_1$ ,  $36^\circ \pm 0.10^\circ$ ; REDUCED FREQUENCY BASED ON SEMI-CHORD,  $k$ , 0.5.

The stability calculations performed for a supersonic airfoil are shown in figure 42. The airfoil was about 5 percent thick, and the results were obtained for a steady-state angle of attack of  $8^\circ$ . Therefore, the results show the effect of both airfoil geometry (thickness and camber) and steady-state angle of attack. The analysis predicts that the airfoil is stable for all interblade phase angles.

**Researchers:** D.L. Huff (NASA Lewis) and T.S.R. Reddy (University of Toledo).

# Concurrent Processing Adaptation of Aeroelastic Analysis of Propfans

An advanced aeroelastic analysis program was adapted to run efficiently on a shared memory multiple processor computer, an Alliant FX/80. The program, ASTROP3, uses a three-dimensional compressible, unsteady aerodynamic model and blade normal modes to calculate aeroelastic stability and response of propfan blades.

Within ASTROP3, the major amount of execution time is used in the computation of aerodynamic influence coefficients. In a representative case with a model of the SR3C-X2 propfan blade, computation of the coefficients uses 97 percent of the total execution time. Fortunately, this computation possesses a very high degree of independence and thus can be done concurrently on separate processors.

The overhead time involved in setting up for vector or concurrent processing must be minimized to achieve efficient execution in a parallel processing environment. Overhead can be controlled by selective use of compiler options and directives to enable vector or concurrent processing only where a reduction in execution time will result. In the ASTROP3 code, changes were made to compute all of the influence coefficients concurrently. Further modifications rescheduled the parallel subtasks such that idle time for available processors was reduced.

Figure 43 presents the speedups attained on the Alliant FX/80 with different numbers of processors for the flutter analysis of an SR3CR-X2 propfan rotor. Also shown in figure 44, for comparison, are the ideal and theoretical speedups. For seven processors,

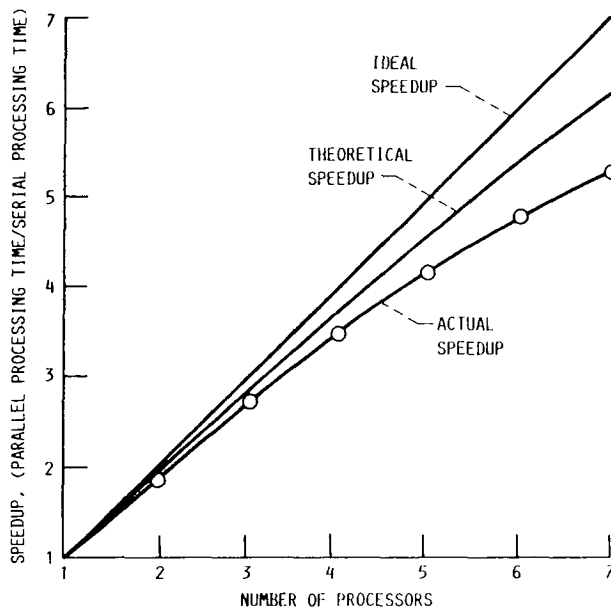


FIGURE 43. - EXECUTION TIME PERFORMANCE OF PARALLEL PROCESSING PROPFAN AEROLLASTIC ANALYSIS.

the actual speedup (parallel processing time/serial processing time) was 5.28, or 75.4 percent of ideal.

**Researchers:** D.C. Janetzke (NASA Lewis) and D.V. Murthy (University of Toledo).

## Flutter Analysis of Supersonic Throughflow Stator

In recent years, interest in providing efficient supersonic propulsion technology for supersonic transport applications has increased. Needless to say, there are major challenges in this effort. One concept which shows considerable promise is the supersonic throughflow fan engine. If successful, this engine will realize a 10-percent increase in installed efficiency and a 25-percent reduction in weight compared with a nonafterburning turbofan engine. The supersonic throughflow fan will efficiently process the intake airflow at supersonic throughflow velocities, thereby eliminating the need for the heavy, conventional supersonic inlet system required by conventional turbomachinery. The SSTF will be about 50-percent lighter in weight than conventional supersonic inlet systems.

The previous research on the SSTF concept is extremely limited. Therefore, to evaluate the concept and potential of an SSTF, NASA Lewis is currently conducting a research effort to design, build, and test an SSTF. During the design of the original rotor blades, the aeroelastic stability became a concern. Consequently, a linear two-dimensional unsteady potential theory code for supersonic axial flow was developed at Lewis and used in conjunction with an existing aeroelastic code MISER2, to perform a flutter analysis. This analysis showed the blades to be unstable; consequently, they were redesigned.

Like the rotor, the aeroelastic stability of the throughflow fan stator also was a concern. The stator was also analyzed for flutter (fig. 44). On this plot of reduced velocity versus Mach number, three curves are shown: flutter boundaries for the stator with 0.0 and 0.3 percent structural damping, respectively, and the torsional mode operating line. If the operating line is above a flutter boundary, the stator is unstable in the torsion mode. If the operating line is below the flutter boundary, the stator is

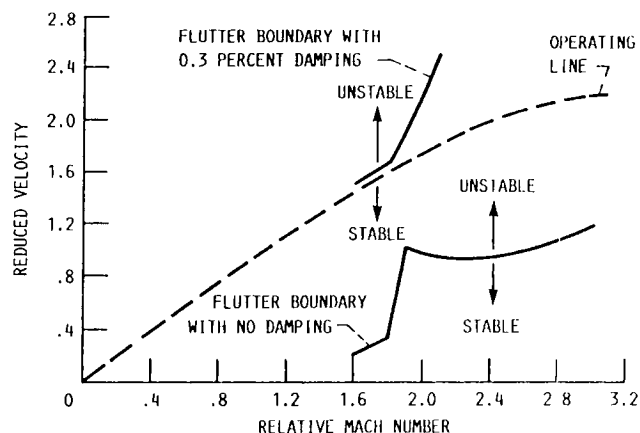


FIGURE 44. - STATOR FLUTTER BOUNDARY.

stable in the torsion mode. As shown in figure 44, the analysis predicted that the stator without structural damping was unstable above relative Mach numbers of 0.5. However, the analysis predicted that the stator with 0.3 percent structural damping was aeroelastically stable. The structural damping associated with the stator will probably be equivalent to or greater than the assumed 0.3 percent used in the analysis. Therefore, we concluded that the original stator design will be aeroelastically stable.

---

**Researchers:** J.K. Ramsey (NASA Lewis) and R.E. Kielb (General Electric).



# Bibliography

- Bakhle, M.A., Keith, T.G. and Kaza, K.R.V.: Application of a Full Potential Solver to Bending-Torsion Flutter in Cascades. 30th Structures, Structural Dynamics and Materials Conference, Part 4, AIAA, 1989, pp. 1982-1990.
- Chung, C.L. and Desa, S.: Global Approach for Using Kinematic Redundancy to Minimize Base Reactions of Manipulators. In: Advances in Design Automation - 1989; ASME, New York, 1989, p. 297-303.
- DellaCorte, C., Steinetz, B.M. and Brindley, P.M.: Tribological Properties of Ceramic/Ti<sub>3</sub>Al-Nb Sliding Couples for Use as Candidate Seal Materials to 700 °C, NASA TM-102401, 1989.
- Farnell, K.E., et al.: User Needs, Benefits and Integration of Robotic Systems in a Space Station Laboratory. (TBE-SSD-P601-89-40), Teledyne Brown Engineering; NASA Contract NAS3-25278), NASA CR-182261, 1989.
- Hucklebridge, A.A.; and Lawrence, C.: Identification of Structural Interface Characteristics Using Component Mode Synthesis, J. Vibration Acoust. Stress Rel. Design, vol. 111, no. 2, Apr. 1989, pp. 140-147.
- Huff, D.L.; and Reddy, T.S.R.: Numerical Analysis of Supersonic Flow Through Oscillating Cascade Sections by Using a Deforming Grid. AIAA Paper 89-2805, July 1989 (NASA TM-102053).
- Kaza, K.R.V., et al.: Analytical Flutter Investigation of a Composite Propfan Model, J. Aircraft, vol. 26, no. 8, Aug. 1989, pp. 772-780.
- Kurkov, A.P.: Optical Measurement of Unducted Fan Blade Deflections. ASME Paper 89-GT-298, June 1989 (NASA TM-100966).
- Lawrence, C.; and Huckelbridge, A.A.: Characterization of Structural Connections Using Free and Forced Response Test Data. NASA TM-101991, 1989.
- Mahajan, A.J.; Dowell, E.H.; Bliss, D.B.: On the Role of Artificial Viscosity in Navier-Stokes Solvers. 9th AIAA Computational Fluid Dynamics Conference, AIAA, 1989, pp. 197-202.
- Murthy, D.V.; and Haftka, R.T.: Approximations to Eigenvalues of Modified General Matrices. Comput. Struct., vol. 29, no. 5, 1988, pp. 903-917.
- Murthy, D.V.: Solution and Sensitivity Analysis of a Complex Transcendental Eigenproblem with Pairs of Real Eigenvalues. NASA CR-182241, 1989.
- Murthy, D.V.; and Kaza, K.R.V.: A Computational Procedure for Automated Flutter Analysis. Commun. Appl. Numer. Methods, vol. 5, no. 1, Jan. 1989, pp. 29-37.
- Quinn, R.; and Lin, N.: New Results Concerning the Use of Kinematically Redundant Manipulators in Microgravity Environments. AIAA Paper 89-3562, Aug. 1989.
- Quinn, R.D.; and Chang, R.K.: Dynamic Modeling of Multi-Jointed Mechanical Systems. Presented at 7th VPI&SU Symposium on Dynamics and Control of Large Structures, Blacksburg, VA, May 8-10, 1989 (to be published).
- Ramsey, J.K.: Influence of Thickness and Camber on the Aeroelastic Stability of Supersonic Throughflow Fans: An Engineering Approach. NASA TM-101949, 1989.

Reddy, T.; and Mehmed, O.: Aeroelastic Analysis of Propfan Blades With a Semi-empirical Dynamic Stall Model. AIAA-89-2695, July 1989.

Savage, M., et al.: Computerized Life and Reliability Modeling for Turboprop Transmissions. J. Propulsion Power, vol. 5, no. 5, Sept.-Oct. 1988, pp. 610-614.

Steinetz, B.M.; DellaCorte, C.; and Sirocky, P.J.: On the Development of Hypersonic Engine Seals. NASA TP-2854, 1988.

Walton, J.; Lee, C.; and Martin, M.: High Speed Balancing Applied to the T700 Engine. (MTI-87TR56, Mechanical Technology, Inc.; NASA Contract NAS3-23929) NASA CR-180899, 1989).



# Report Documentation Page

<b>1. Report No.</b> NASA TM-102488	<b>2. Government Accession No.</b>	<b>3. Recipient's Catalog No.</b>	
<b>4. Title and Subtitle</b> Structural Dynamics Branch Research and Accomplishments for FY 1989		<b>5. Report Date</b> July 1990	
		<b>6. Performing Organization Code</b>	
<b>7. Author(s)</b>		<b>8. Performing Organization Report No.</b> E-5279	
		<b>10. Work Unit No.</b> 505-63-1B	
<b>9. Performing Organization Name and Address</b> National Aeronautics and Space Administration Lewis Research Center Cleveland, Ohio 44135-3191		<b>11. Contract or Grant No.</b>	
		<b>13. Type of Report and Period Covered</b> Technical Memorandum	
<b>12. Sponsoring Agency Name and Address</b> National Aeronautics and Space Administration Washington, D.C. 20546-0001		<b>14. Sponsoring Agency Code</b>	
		<b>15. Supplementary Notes</b>	
<b>16. Abstract</b>  This publication contains a collection of fiscal year 1989 research highlights from the Structural Dynamics Branch at NASA Lewis Research Center. Highlights from the branch's major work areas—Aeroelasticity, Vibration Control, Dynamic Systems, and Computational Structural Methods—are included in the report as well as a listing of the fiscal year 1989 branch publications.			
<b>17. Key Words (Suggested by Author(s))</b> Aeroelasticity Vibration control Dynamic systems		<b>18. Distribution Statement</b> Unclassified - Unlimited Subject Category 39	
<b>19. Security Classif. (of this report)</b> Unclassified	<b>20. Security Classif. (of this page)</b> Unclassified	<b>21. No. of pages</b> 50	<b>22. Price*</b> A03